Journal of proteome research

Article

Cite This: J. Proteome Res. 2018, 17, 3195−3213

pubs.acs.org/jpr

Development of in Planta Chemical Cross-Linking-Based Quantitative Interactomics in *Arabidopsis*

Shichang Liu,[†,○] Fengchao Yu,[‡,§,○] Qin Hu,[†] Tingliang Wang,[∥] Lujia Yu,[#] Shengwang Du,[⊥,#] Weichuan Yu,[*,‡,§] and Ning Li[*,†,‡,▽]

[†]Division of Life Science, Energy Institute, Institute for the Environment, The Hong Kong University of Science and Technology, Hong Kong SAR, China

[‡]Division of Biomedical Engineering, The Hong Kong University of Science and Technology, Hong Kong SAR, China

[§]Department of Electronic and Computer Engineering, The Hong Kong University of Science and Technology, Hong Kong SAR, China

[∥]Tsinghua-Peking Joint Center for Life Sciences, Center for Structural Biology, School of Life Sciences and School of Medicine, Tsinghua University, Beijing 100084, China

[⊥]Department of Physics, The Hong Kong University of Science and Technology, Hong Kong SAR, China

[#]Department of Chemical and Biological Engineering, The Hong Kong University of Science and Technology, Hong Kong SAR, China

[▽]The Hong Kong University of Science and Technology, Shenzhen Research Institute, Shenzhen Guangdong 518057, China

Supporting Information

ABSTRACT: An in planta chemical cross-linking-based quantitative interactomics (IPQCX−MS) workflow has been developed to investigate in vivo protein−protein interactions and alteration in protein structures in a model organism, *Arabidopsis thaliana*. A chemical cross-linker, azide-tag-modified disuccinimidyl pimelate (AMDSP), was directly applied onto *Arabidopsis* tissues. Peptides produced from protein fractions of CsCl density gradient centrifugation were dimethyl-labeled, from which the AMDSP cross-linked peptides were fractionated on chromatography, enriched, and analyzed by mass spectrometry. ECL2 and SQUA-D software were used to identify and quantitate these cross-linked peptides, respectively. These computer programs integrate peptide identification with quantitation and statistical evaluation. This workflow eventually identified 354 unique cross-linked peptides, including 61 and 293 inter- and intraprotein cross-linked peptides, respectively, demonstrating that it is able to in vivo identify hundreds of cross-linked peptides at an organismal level by overcoming the difficulties caused by multiple cellular structures and complex secondary metabolites of plants. Coimmunoprecipitation and super-resolution microscopy studies have confirmed the PHB3−PHB6 protein interaction found by IPQCX−MS. The quantitative interactomics also found hormone-induced structural changes of SBPase and other proteins. This mass-spectrometry-based interactomics will be useful in the study of in vivo protein−protein interaction networks in agricultural crops and plant−microbe interactions.

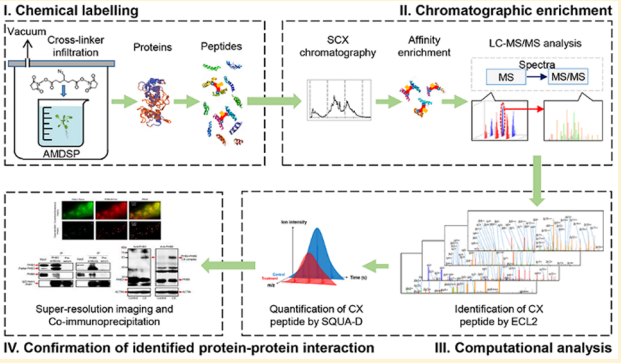

KEYWORDS: *IPQCX−MS, in planta quantitative interactomics, in vivo cross-linking, ECL2, 4C proteomic workflow, Arabidopsis thaliana*

INTRODUCTION

The dynamic and physical interactions of proteins are involved in various cellular processes, ranging from DNA replication, transcription, translation, signal transduction, enzyme activities, and channel opening and closing to metabolism.[1] These interactions determine the behavior of an organism or a biological system.[2,3] The proteome-wise profiling of the cellular protein−protein interaction helps to delineate the molecular mechanisms underlying various cellular events.

To investigate protein−protein interactions, numerous in vitro and in vivo approaches have been established previously.[4,5] These methods include yeast two-hybrid assay,[6] affinity purification−mass spectrometry (AP−MS),[7] protein microarray,[8] bimolecular fluorescence complementation (BiFC),[9] split luciferase complementation assay,[10] fluorescence resonance energy transfer (FRET),[11] bioluminescence resonance energy transfer (BRET),[12] and several proximity-dependent labeling methods, such as engineered ascorbate peroxidase (APEX)[13] and proximity-dependent biotin identification

Received: May 8, 2018
Published: August 7, 2018

DOI: 10.1021/acs.jproteome.8b00320
J. Proteome Res. 2018, 17, 3195−3213

(BioID).[14,15] The proximity-dependent labeling methods can map both stable and transient protein−protein interactions by fusion of an enzyme to a target protein to label the proximate proteins (e.g., biotin labeling). The tag-labeled proteins or peptides can be enriched by affinity purification and identified by MS.[5] Chemical cross-linking coupled to mass spectrometry (CX−MS) has recently emerged as an alternative means to study protein topology[16−18] and has become increasingly useful in providing direct evidence of protein−protein interactions at the whole proteome level.[18−20] The chemical cross-linking of two proteins is generally achieved by joining moieties of two polypeptides via a bifunctional chemical with two reactive ends.[21] The membrane-permeable disuccinimidyl suberate (DSS)-H12/D12 is a frequently used cross-linker.[17,19] The cross-linked proteins are first processed by proteases, consequently enriched for MS analysis, and finally identified using computational programs.[17,19] These CX−MS data containing the protein topology information have been used to complement the 3D structural data derived from X-ray crystallography, nuclear magnetic resonance (NMR), and cryo-electron microscopy (cryo-EM) in the study of the dynamics of protein complexes.[22,23]

To advance the MS-based study of protein−protein interaction networks in vivo, membrane-permeable, affinity column-enrichable, and MS-cleavable cross-linkers, such as the protein interaction reporter (PIR[24]), have been employed in the study of CX−MS-based interactomics.[25,26] Similarly, this cross-linker has been applied in the investigation of inter-species protein−protein interactions during bacterial infection.[27] An azide-tagged, acid-cleavable disuccinimidyl bis-sulfoxide (azide-A-DSBSO), which is also a membrane-permeable, enrichable, and MS-cleavable cross-linker, has been applied to identify in vivo protein−protein interactions in HEK 293 cells on both the whole proteome scale and in the targeted proteasome complexes.[28] Moreover, at the animal tissue level,[29] Chavez et al. reported a chemical cross-linking-based interactomics on minced mice heart tissues to map out the protein structures and protein−protein interactions.[30] However, the application of CX−MS in plant tissue is quite difficult, and, so far, only a few cross-linked peptides have been identified[31] because of the interference of complex secondary metabolites in plants, which usually contain over 100 amine-contained secondary metabolites.[32] These amines may titrate the penetrated *N*-hydroxysuccinimide (NHS) ester-containing cross-linker.

The cross-linkers used in CX−MS have generally been classified into MS-noncleavable[19] and MS-cleavable;[28] MS-noncleavable cross-linkers have a relatively long history (Table S1) and have been widely applied and well studied. A significant number of studies have used noncleavable cross-linkers, such as DSS and bis(sulfosuccinimidyl)suberate (BS3), to study protein structures[19,33−36] and protein−protein interactions.[37−39] Because of their straightforward experiment protocols, as compared with those of MS-cleavable cross-linkers, such MS noncleavable cross-linkers are still used in biological studies[31] today. Along with these MS noncleavable cross-linkers, many computational programs have been developed (Table S1). The typical software includes xQuest/xProphet,[40,41] pLink,[42] Kojak,[43] ECL,[44,45] and so on. All of these tools apply sophisticated algorithms to identify cross-linked peptides with a high sensitivity and specificity (Table S1).

In contrast with MS-noncleavable cross-linkers, MS-cleavable cross-linkers have only recently been developed[28,46−48] to address the quadratic search space issue often encountered during the application of MS-noncleavable cross-linkers in CX−MS interactomics. In the analysis of MS-cleavable cross-linker-mediated cross-linked peptides, two dissociation steps produce three levels of mass spectrograms (i.e., MS^1, MS^2, and MS^3). At the end of MS analysis, each cross-linked peptide ion produces two MS^3 spectra from the fragmentation of two peptide chains. As a result, the cross-linked peptide identification problem is converted to a linear peptide identification problem. Furthermore, Liu et al.[49] proposed a method to avoid using MS^3 in analyzing MS-cleavable cross-linker-conjugated peptides. Thus two computational programs[49,50] have been applied to identify cross-linked peptides linked by MS-cleavable cross-linkers.

To quantitate cross-linked peptides, either a label-free or an isotope-labeled cross-linker-based CX−MS approach has been adopted. The quantified conformational changes of protein complexes include F-type ATPase isolated from spinach leaves,[51] proteasome purified from yeast,[52] commercial bovine serum albumin (BSA), bovine transferrin, chicken ovotransferrin,[53] and commercial plasma of human C3 cells.[54] The label-free quantitation strategy was applied in a study of the interaction between calmodulin and its substrates,[55] whereas a method that integrates PIR-based in vivo cross-linking with SILAC-based quantitative proteomics was successfully introduced to measure protein conformational changes and interaction networks between drug-sensitive and drug-resistant HeLa cells.[56] Chavez et al. developed a method that combines both MS1-based and targeted-MS2 (parallel reaction monitoring, PRM)-based quantitation to study how drugs affect the in vivo conformational dynamics and interactions of cytosolic heat shock protein Hsp90 in HeLa cells.[22] However, quantitative in planta CX−MS interactomics has not been reported so far.[31]

To develop quantitative CX−MS-based interactomics, a relatively quantitative method, dimethyl-labeling-based quantitative proteomics,[57−59] has been integrated with the CX−MS approach. Dimethyl labeling generally achieves 99% labeling efficiency.[60] Although other MS^1-based (e.g., ICAT labeling[61]) and MS^2-based quantitative proteomics (e.g., iTRAQ[62] and TMT labeling[63]) as well as label-free quantitative proteomics have been applied in the study of organisms unavailable for cultivation in the isotope-coded growth medium, dimethyl-labeling-based peptide quantitation, in contrast, is quite useful in the study of proteomes of a mouse cell line,[64] human cell lines,[65,66] *Arabidopsis*,[67] rat organs,[68] and human liver tissue.[69] It has also been useful in quantitating post-translationally modified proteins.[70−73] Moreover, Cheng et al. applied dimethyl labeling in combination with in vitro AP−MS to quantify and identify 17β-estradiol-induced components' changes in the estrogen response element (ERE) complex of MCF-7 cells.[74] Lau et al. applied a similar strategy to quantitatively map interactors of the SH2 domain of human growth receptor-bound protein 2 (GRB2) in HeLa cells.[75]

In the present study, we integrate isotopic dimethyl-labeling-based peptide quantitation with in planta CX−MS.[31] This new strategy significantly increases the total number of in vivo cross-linked peptides and establishes a quantitative in planta CX−MS approach, named in planta quantitative cross-linking coupled mass spectrometry (IPQCX−MS). The IPQCX−MS interactomics workflow is abbreviated as a "4C interactomic workflow." The "C" is derived from the first English letter in the title of each step of the IPQCX−MS, comprising chemical labeling (i.e., in vivo protein cross-linking and in vitro isotopic dimethyl labeling of peptides), chromatographic enrichment (i.e., strong cation exchange−high-performance liquid chromatography

DOI: 10.1021/acs.jproteome.8b00320
J. Proteome Res. 2018, 17, 3195−3213

(SCX-HPLC), affinity purification of cross-linked peptides, and C18-HPLC coupled MS/MS analysis), computational program analysis using updated ECL2 software, and confirmation of identified cross-linked peptides with alternative methods. This 4C interactomics workflow is able to investigate in vivo protein−protein interactions and protein structures at a multicellular organismal level of plants. To increase the identification of cross-linked peptides from the in planta cross-linked whole proteome, we designed and synthesized a membrane-permeable and enrichable in vivo cross-linker, azide-tag modified disuccinimidyl pimelate (AMDSP), which has two reactive NHS esters at two ends, with an additional azidomethyl group on the spacer chain of this cross-linker. This azide-tagged cross-linker is accessible to the click reaction for conjugation with a biotin tag, which allows subsequent chromatography enrichment of cross-linked peptides.[28,76] The cross-linked peptides were subsequently analyzed using a new computational program named ECL2.[45] ECL2 advances the state-of-the-art tools[40,42,43] with the ability to exhaustively check all possible peptide−peptide pairs with linear time complexity. We also used pLink[42] and Kojak[43] to analyze our data set. The result showed that ECL2 identified the most cross-linked peptides, which is consistent with the conclusions reported by Yu et al.[45]

EXPERIMENTAL SECTION

Synthesis of Cross-Linker AMDSP and Chemical Compound DLBA

Bis(2,5-dioxopyrrolidin-1-yl)4-(azidomethyl) heptanedioate is an azide-tag-modified disuccinimidyl pimelate (AMDSP, Figure 1C and Figure S1) chemical compound that was custom synthesized by AQ BioPharma (Shanghai, China), whereas *N*-(2-((3-oxo-3-(prop-2-yn-1-yl amino)proyl)disulfanyl)ethyl)-5-((3a*S*,4*S*,6a*R*)-2-oxohexahydro-1*H*-thieno [3,4-*d*]imidazole-4-yl) pentanamide, commonly called disulfide-linked biotin and alkyne (DLBA, Figure 1C and Figure S2), was custom-synthesized by Medi-tech Bioscientific (Changzhou, China).

In Vitro Chemical Labeling of Synthetic Peptides

Synthetic peptides of Fmoc-EAKELIEGLPR and Fmoc-KELDDLR were synthesized by Minghao Biotechnology (Wuhan, China). Fmoc-protected N-terminal amine promotes the cross-linking between two peptides at the side chains of lysine. The AMDSP-based cross-linking of two synthetic peptides followed a previously described method.[31] The cross-linked peptides were labeled with CH_2O and $NaBH_3CN$ (in 1 M NaOH) to produce dimethyl groups on synthetic peptides using a method described by Boersema et al.[58] After the cross-linked peptides were desalted on an Oasis HLB (hydrophilic−lipophilic-balanced) 1 cc cartridge (Waters, Milford, MA), they were resuspended in 50 mM 4-(2-hydroxyethyl)-1-piperazineethanesulfonic acid (HEPES, pH 7.5) at room temperature for 2 h to perform the click reaction. DLBA of 5 mM was added as a reactant, and 1 mM $CuSO_4$ and sodium ascorbic acid each were added as catalysts in the click reaction. Tris[(1-benzyl-1*H*-1,2,3-triazol-4-yl) methyl] amine (TBTA, 100 μM) was added to the reaction to stabilize the generated univalent copper. Consequently, a high-performance liquid chromatography (HPLC) system (Waters 600 Controller, Water Delta 600 Pump, and Water 2487 Dual λ Absorbance Detector, Waters) coupled to a 200 × 4.6 mm SCX column (PolySULFOETHYL ATM, 5 μm, 200 Å, PolyLC, USA) was applied to remove the excess DLBA. The remaining cross-linked peptides were collected and enriched again with an HLB cartridge. The cross-linked peptides were pulled down with high-capacity streptavidin agarose resin (Pierce, Rockford, IL). After 2 h of incubation, 50 mM of tris(2-carboxyethyl) phosphine (TCEP) was used to cleave the disulfide bond on the DLBA. The cross-linked peptides were eluted off the agarose resin to be enriched with a C18 ZipTip (Millipore, Billerica, MA). Consequently, the free thiol group of the cross-linked peptides was blocked by iodoacetamide (IAM), and the peptides were subsequently analyzed using LC−MS/MS. To verify the success of each step of the chemical reactions (Figure 1C), the intermediate and the ultimate cross-linked synthetic peptides were identified using MS (Figure S3). The data on cross-linked peptides were used to test ECL2 (Figure 1C and Figure S3D).

Plant Growth and Hormone Treatment

The seeds of the wild-type *Arabidopsis thaliana* ecotype *Columbia-0* (*Col-0*) and the T-DNA insertional mutants, SALK_020707 (insertion in AT5G40770, *phb3*, see FigureS5A for validation) and CS858159 (insertion in AT2G20530, *phb6*, see Figure S5B for validation) were purchased from the *Arabidopsis* Biological Resource Center (ABRC, Columbus, OH). The seeds of double-mutants *ein3/eil1* were gifts from Dr. Hongwei Guo at the Southern University of Science and Technology. *Arabidopsis* plants were grown on 50 mL of Murashige and Skoog (MS) basal agar medium in transparent white glass jars of 7.7 cm diameter and 12.7 cm height. Ethylene hormone treatment was performed by adding ethylene precursor, 10 μM 1-amino-cyclopropane-1-carboxylic acid (ACC), into the agar medium.[77] The growth conditions were controlled at 23.5 ± 1 °C, with a growth regime of 16 h of light (210 ± 30 μE m^{-2} s^{-1}) and 8 h of darkness. *Arabidopsis* plants of *Col-0*, *ein3/eil1*, *phb3*, and *phb6* genotypes were grown in glass jars with a density of three plants per jar and used for phenotype measurements on the 38th day. In a single biological replicate of the IPQCX−MS experiment, the in planta chemical cross-linking was performed on ∼2000 individuals of 21 day old *ein3/eil1* plants. A total of three biological replicates were performed for the interactomics.

In Planta Chemical Cross-Linking

The chemical cross-linking buffer was modified from methods described previously.[31,78] The 21 day old plants were immersed in an in planta cross-linking buffer (1.76 mM KH_2PO_4, 10 mM Na_2HPO_4, 136 mM NaCl, 2.6 mM KCl, 0.1% formaldehyde, 8% DMSO, and 10% glycerol, pH 8.0). The 50 mM AMDSP was made using DMSO and diluted in a working concentration of 1 mM in the in planta cross-linking buffer. The cross-linker was infiltrated into plant cells through five cycles of pressure shift between the atmospheric pressure and a pressure of 600 Torr within 30 min.[31] The cross-linking reactions were quenched with 50 mM NH_4HCO_3. The cross-linked tissues were washed three times with double-distilled water and harvested with liquid nitrogen. The harvested tissues were ground into frozen powder using a ceramic mortar and pestle and subsequently stored at −80° C for the next step of protein extraction.[31] The effectiveness of this type of in vivo cross-linking was accessed subsequently using immunoblot measurement of the mass shift of cross-linked actin proteins.[31]

Cesium Chloride Density Gradient Centrifugation Fractionation of Proteins

The total cellular proteins were extracted from both the control and the treated tissues using four volumes of detergent-free and urea-based CsCl density gradient (CDG) protein extraction buffer.[31,79] Centrifugation was performed at 218 000*g* for 120 min

DOI: 10.1021/acs.jproteome.8b00320
J. Proteome Res. 2018, 17, 3195−3213

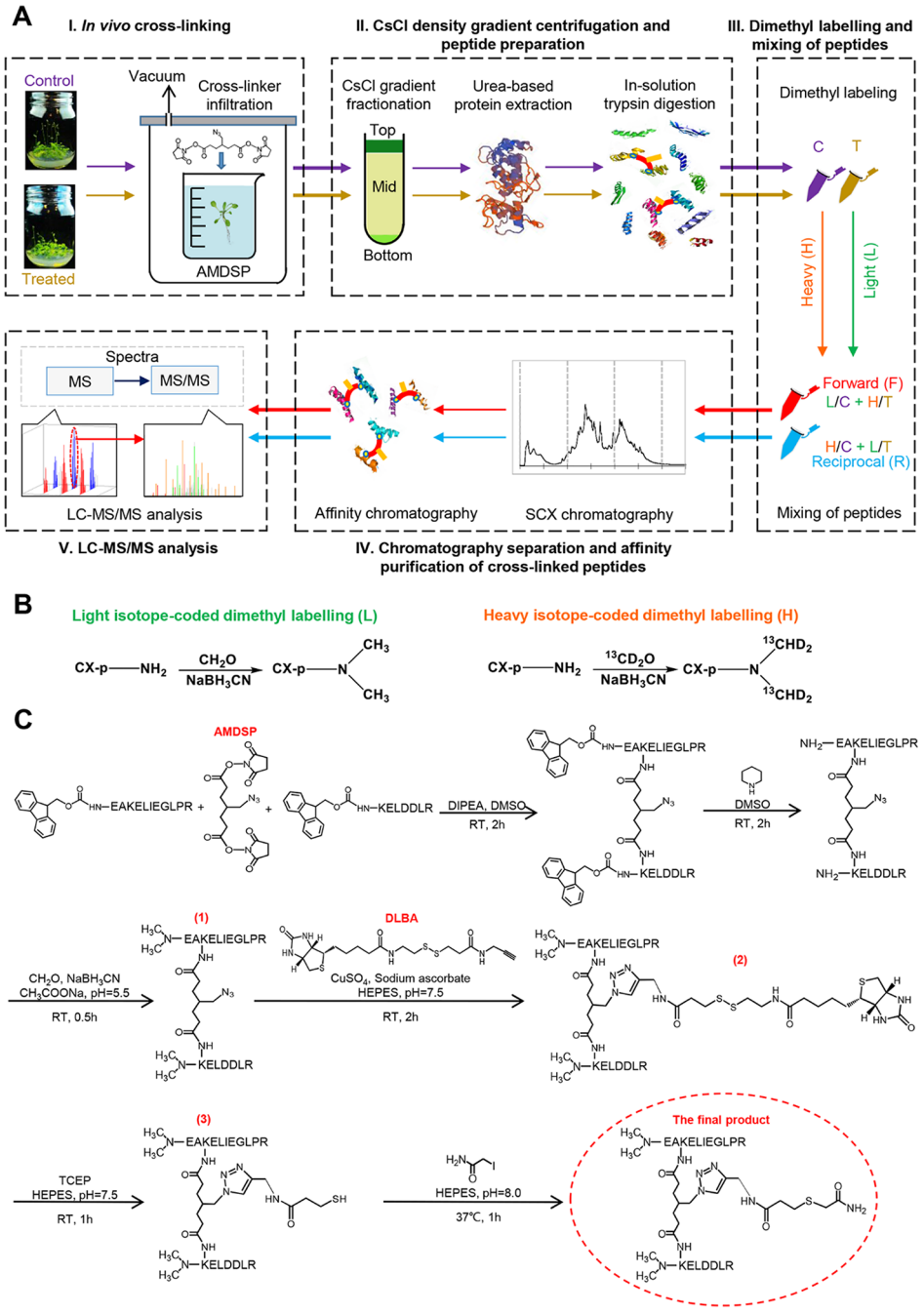

Figure 1. Chemical labeling of *Arabidopsis* proteomes and chromatography enrichment for LC−MS/MS analysis of cross-linked peptides. (A) Workflow of in planta chemical cross-linking of the complete plant proteome, fractionation of proteins by CsCl density gradient centrifugation, and peptide preparation, chromatography enrichment, and LC−MS/MS analysis of cross-linked peptides. AMDSP denotes azide-modified disuccinimidyl pimelate. Multiple vacuum infiltration was applied to whole plants submerged in AMDSP solution. The total cellular proteins of *Arabidopsis* were separated into top (t), middle (m), and bottom (b) fractions. The peptides generated from control (C) and treated (T) *Arabidopsis* proteomes in the top, middle, and bottom fractions were chemically labeled as either light- (i.e., 28 Da) or heavy- (i.e., 34 Da) isotope-labeled dimethyl modifications, respectively. The mixtures of light-isotope-labeled cross-linked peptides from the control samples and heavy-isotope-labeled cross-linked peptides from the treated samples were defined as forward (F) replicates, while the mixtures of heavy-isotope-labeled cross-linked peptides from the control samples and light-isotope-labeled cross-linked peptides from the treated samples were defined as reciprocal (R) replicates. A biological experiment produced both F and R replicates. tF, tR, mF, mR, bF, and bR denote F and R replicates derived from top, middle, and bottom protein fractions, respectively. The peptide mixtures were subjected to the click reaction and separated using SCX-HPLC, followed by biotin−streptavidin affinity chromatography enrichment and LC−MS/MS analysis. The chemical labeling scheme and chromatography workflow are shown in Figure S6A. (B) Chemical structure of light- and heavy-isotope-labeled dimethyl modifications; the labeling reaction of the N-terminal and lysine side chain of the cross-linked peptides (CX-p). A cross-linked peptide consists of α and β peptides. (C) Chemical reaction procedure to produce the AMDSP cross-linked synthetic peptides: EAKELIEGLPR and KELDDLR. DIPEA denotes *N*,*N*-diisopropylethylamine. RT denotes room temperature. DLBA was conjugated to AMDSP-cross-linked synthetic peptides through the click reaction. Cross-linked peptides were enriched with streptavidin agarose and eluted by tris(2-carboxyethyl) phosphine (TCEP). The free thiol group of the cross-linked peptides was blocked with iodoacetamide (IAM). The MS^2 spectra of cross-linking intermediates and the final product of cross-linked synthetic peptides are shown in Figure S3.

DOI: 10.1021/acs.jproteome.8b00320
J. Proteome Res. 2018, 17, 3195−3213

at 10 °C to separate the total cellular protein into top (t), middle (m), and bottom (b) protein fractions. The membrane proteins associated with fraction t and b were solubilized in five volumes of a membrane-solubilizing and protein-denaturing (MSPD) buffer containing 20 mM Tris-HCl (pH 7.8), 8 M urea, 10 mM EDTA, 10 mM EGTA, 50 mM NaF, 2% glycerol, 1% glycerol-2-phosphate disodium salt hydrate, 1 mM PMSF, 1% sodium dodecyl sulfate (SDS), and 1.2% Triton-X100. The extracted protein fractions t, m, and b were precipitated by an acetone and methanol mixture (v/v 12:1), resuspended in the urea-based protein resuspension buffer,[77] and quantified by a DC protein assay kit (Bio-Rad, Hercules, CA) according to previously described methods.[80]

Protein Digestion, Dimethyl Labeling, and Peptide Mixing

Proteins were digested by trypsin protease (Promega, Madison, WI) as previously described.[31] Following the desalting, the digested peptides were enriched using C18 Sep-Pak cartridges (Waters, United Kingdom), and the peptides of the control and ethylene-treated plants were separated into two aliquots, half of which were labeled with light (L)-isotope-coded chemicals ($^{12}CH_2O$ and $NaBH_3CN$), while the other half were labeled with heavy (H)-isotope-coded dimethyl chemicals ($^{13}CD_2O$ and $NaBH_3CN$) in the presence of 100 mM sodium acetate (pH 5.5).[58,77] Both L- and H-peptides derived from the control and the treated plants, respectively, were combined to produce three mixtures (or called pairs) of peptides and defined subsequently as forward (F)-mixing experimental replicates, that is, tF, mF, and bF. Conversely, the H- and L-peptides derived from the control and the treated plants, respectively, were combined to produce three pairs of reciprocal (R) experimental replicates, that is, tR, mR, and bR.

Conjugation of Cross-Linked Peptides with DLBA via Click Chemistry

Peptides desalted on a C18 Sep-Pak cartridge (WAT020515, Waters) were dissolved in 50 mM of HEPES (pH 7.5) to make a final concentration of 4 mg/mL. A click reaction was performed in a peptide solution, containing 0.5 mM DLBA, 0.5 mM $CuSO_4$, 0.5 mM sodium ascorbate, and 0.1 mM TBTA, for 2 h at room temperature.[76]

Chromatographic Separation, Affinity Enrichment, and Chemical Modification of Cross-Linked Peptides

The six peptide samples (derived from three CDG protein fractions (t, m, b) × two types of mixings (F and R)) were dissolved in a mobile phase solution for the subsequent SCX-HPLC separation. Mobile phase A contained 7 mM KH_2PO_4 (pH 2.7) and 30% acetonitrile, and mobile phase B contained 7 mM KH_2PO_4 (pH 2.7), 350 mM KCl, and 30% acetonitrile. Each peptide sample was separated into three subfractions using a 200 × 9.4 mm SCX column (PolySULFOETHYL ATM, 5 μm, 200 Å, PolyLC, Columbia, MD) at a flow rate of 2.5 mL/min. The elution gradient was established as follows: 0−10 min 0−10% B, 10−27 min 10−17% B, 27−40 min 17−32% B, 40−50 min 32−60% B, 50−52 min 60−100% B, 52−60 min 100−0% B, 60−90 min 0% B.[81] Ultraviolet absorption at 214 nm was applied to monitor the eluate. A total of 18 HPLC-fractionated peptide samples (9 from F mixing and 9 from R mixing) were eventually produced from a single biological replicate.

The cross-linked peptides were purified by incubating the HPLC-fractionated peptides with a high-capacity streptavidin agarose resin (Pierce) for 2 h to enrich the biotin-tagged and cross-linked peptides. After washing the agarose resin thoroughly with a washing buffer (50 mM HEPES, 0.05% SDS, pH 7.5), 50 mM TCEP reductant was applied to the resin to cleave the disulfide bound between the biotin and cross-linker to release the cross-linked peptides into solution. The reaction was performed for 2 h. The free thiol moiety of the cross-linked peptides was then blocked by 20 mM of IAM for later LC−MS/MS analysis.

Liquid Chromatography−Tandem Mass Spectrometry (LC−MS/MS) Analysis

Both the final product of cross-linked synthetic peptides and the cross-linked plant peptides were injected into an LC−MS/MS machine, consisting of a Dionex UltiMate 3000 UHPLC and a Q Exactive Hybrid Quadrupole-Orbitrap Mass Spectrometer (Thermo Fisher Scientific, San Jose, CA). A gradient elution was performed on a MonoCap capillary monolith HPLC column (0.1 × 2000 mm, GL Science, Shinjuku-ku, Tokyo) with a flow rate of 0.4 μL/min for 220 min. Mobile phase A consisted of 0.1% formic acid, while mobile phase B consisted of 80% acetonitrile and 0.08% formic acid. The gradient was established as follows: 0−13 min 4% B, 13−14 min 4−8% B, 14−80 min 8−25% B, 80−130 min 25−55% B, 130−150 min 55−99% B, 150−190 min 99% B, 190−192 min 99−4% B, and 192−220 min 4% B. The data-dependent acquisition mode was used to generate the MS data. The normalized collision energy was set at 28% (HCD). In each cycle, the mass spectrometer generated one full scan (300−1800 m/z, 70 000 resolution), followed by 20 MS/MS scans with a resolution of 17 500. The isolation window was 2.0 Da, while the dynamic exclusion duration was 5 s. The charge range was from +3 to +8.

Computational Analysis of Mass Spectrometry Data

The raw MS data were first converted into the mzXML format using ProteoWizard (version: 3.0.11110 64-bit).[82] The converted MS/MS data were consequently analyzed using Mascot (version 2.5.0) to search against the target and decoy TAIR10 *Arabidopsis* protein databases, which currently contain 35 387 protein sequences (https://www.arabidopsis.org/download_files/Sequences/TAIR10_blastsets/TAIR10_pep_20101214_updated), respectively. The precursor mass tolerance was set at 10 ppm, while the MS/MS mass tolerance was set at 0.01 Da. Trypsin was selected as protease, while the maximum allowed number of missed cleavages was set at 2. Because monolinks were set as 397.165799 and 398.149815 Da on residue (K) and N-terminus, respectively, they were set as the variable modifications. Because both light (28.031300 Da) and heavy isotopic dimethyl (34.063117 Da) were used to label lysine residues and N-termini of peptides, they were set as the variable modifications on lysine and the N-termini of peptides. Oxidation on methionine was set as the variable modification. We also set carbamidomethyl (57.021464 Da) on cystine (C) as the fixed modification. The false discovery rate (FDR) ≤ 0.01 was used to select peptide-spectrum matches (PSMs) from the results of the Mascot search. Normally, researchers convert the FDR estimated based on the target-decoy strategy into a q value for its monotonicity and higher power. In this study, we always convert the FDR into a q value and use the q value in the cutoff. To avoid confusion, we still refer to this value as FDR to be consistent with other researchers. From 77 226 identified PSMs (Table S2a), there were 5538 proteins, which were used to generate a custom protein database of smaller size for the following ECL2 (version 2.1.7)-based cross-linked peptide identification. The precursor mass tolerance was set at 10 ppm. The MZ bin size was set at 0.02, which corresponds to

DOI: 10.1021/acs.jproteome.8b00320
J. Proteome Res. 2018, 17, 3195−3213

MS/MS mass tolerance being set at 0.01 Da. FDR for PSM was set as ≤ 0.05.

The mass spectrometry data have been deposited to the ProteomeXchange[83] Consortium via the PRIDE[84] partner repository with a data set identifier PXD008161.

Quantitation of cross-linked peptides was performed using the extracted ion chromatogram (XIC)-based SQUA-D (version 2.0) software as previously described.[77] In the analysis, we selected the quantifiable cross-linked peptide ions according to the following criteria:

(1) The PSM number of light-dimethyl-labeled cross-linked peptides is ≥ 1.
(2) The PSM number of heavy-dimethyl-labeled cross-linked peptides is ≥ 1.
(3) The total PSM number obtained from at least three out of six independent experimental replicates should be ≥ 3.
(4) The number of identified PSMs of a peptide from the forward experiments divided by the total number of its corresponding PSMs is ≥ 0.20.
(5) The number of identified PSMs of a peptide from the reciprocal experiments divided by the total number of its corresponding PSMs is ≥ 0.20.

The criteria used to select significantly altered cross-linked peptides are as follows: |fold-change| ≥ 1.5 (or |log-ratio| ≥ 0.58) and BH-FDR (Benjamini–Hochberg multiple test correction) ≤ 0.1.

Bioinformatic Analysis

The database used for the gene ontology (GO) analysis of protein was downloaded from the TAIR website. GO analysis was performed using the following equation

$$R_i = \log_2\left(\frac{N_i/N}{N_i'/N'}\right)$$

where N is the total match number of all categories of the cross-linked proteins, N' is the total match number of all categories of the leaf proteome of *Arabidopsis*,[85] N_i is the match number of the cross-linked proteins belonging to the ith category, and N_i' is the match number of proteins from the leaf proteome of *Arabidopsis* belonging to the ith category. The top three categories sorted by fold enrichment were selected.

The bioinformatics tool used in GO enrichment analysis is the Database for Annotation, Visualization and Integrated Discovery (DAVID) version 6.7 (https://david-d.ncifcrf.gov/tools.jsp). The thresholds were set as the following: gene count ≥ 5, P value ≤ 0.01, and FDR ≤ 0.1.

Protein-Modeling and Protein–Protein Interaction Analysis

Protein modeling was performed using an online software I-TASSER.[86] For each protein, the model of the highest C-score was selected. Docking of interacting proteins was assessed using the online software PatchDock[87] with the following parameters: The clustering root-mean-square deviation (RMSD) is 4.0 and the complex type is default. The distance between two cross-linked lysines was set to be within 20 Å. The 3D structures of the proteins were drawn using the software ICM-Browser 3.8. The identified protein–protein interactions were searched using STRING 10.5 (https://string-db.org/) and software *Arabidopsis* Interactions Viewer (http://bar.utoronto.ca/interactions/cgi-bin/arabidopsis_interactions_viewer.cgi). The *Arabidopsis* Interactions Viewer is a database that includes 36 352 confirmed and 70 944 predicted *Arabidopsis* interacting proteins.

Antibody Production and Immunoblot Assays

Rabbit polyclonal antibodies were raised against the $_{157}$ESL-ITRAKDFNIVL peptide of prohibitin 3 (PHB3, AT5G40770) and $_{48}$RLVGIKDKVYPEGT peptide of prohibitin 6 (AT2G20530), respectively, by GL Biochem (Shanghai, China). The anti-PIP2a rabbit polyclonal antibody was raised in our laboratory.[80] The antiactin (plant) monoclonal antibody (a0480) was purchased from Sigma-Aldrich (St. Louis, MO). Protein extraction and immunoblotting were performed as previously described.[80]

Coimmunoprecipitation

The coimmunoprecipitation was performed at 4 °C, as previously described.[88] Protein extraction buffer, containing 50 mM Tris-HCl, 100 mM NaCl, 1 mM EDTA, 0.1% Triton X-100, 10% glycerol, 2 mM PMSF, and 2× EDTA-free protease inhibitor cocktail (Complete Roche), was used to lyse plant cells. Following centrifugation, the supernatant of cell lysate was incubated with antibody-coupled beads for 1 h. The protein complexes were enriched with antibodies and eluted with a buffer containing 50 mM Tris-HCl (pH 6.8), 8 M urea, 5 mM dithiothreitol (DTT), 1% SDS, and 10 mM EDTA.

Plant Tissue Section Preparation and Immunostaining

To prepare *Arabidopsis* tissue sections for immunostaining,[89] photobleaching (1000 W halogen projector lamp with intensity of 1800 μmol photons m^{-2} s^{-1}) was performed first in 2% BSA solution for 1 h. Sections of *ein3/eil1* plant tissues were incubated with anti-PHB6 polyclonal antibody for 12 h at 4 °C. After washing the plant tissue sections with the microtubule-stabilizing (MTSB) buffer, containing 50 mM piperazine-*N*,*N*′-bis[2-ethanesulfonic acid] (PIPES), 5 mM $MgSO_4$, and 5 mM EGTA (pH 6.9), three times (10 min per washing), these sections were incubated with goat antirabbit IgG (H+L), Alexa Fluor 647 (Thermo Fisher Scientific) for 5 h at 4 °C. Following the first immunostaining with anti-PHB6 polyclonal antibody and secondary antibody conjugated with Alexa Fluor 647 dye, these prestained sections were washed again with MTSB buffer three times and with 10 min of washing per round. The anti-PHB3 polyclonal antibody conjugated to Alexa Fluor 750 dye (Molecular Probes; Invitrogen, Eugene, OR) was then added consequently to locate the PHB3. These two different immune-labeling dyes were also applied to conjugate PHB3/PHB6 and water channel protein PIP2a. The polyclonal anti-PIP2a antibody was conjugated with Alexa Fluor 750, which was used to analyze colocalization coefficients of aquaporin and PHB3/6 proteins.

To test the specificities of anti-PHB3 and anti-PHB6 antibodies, immunostaining was performed on *Col-0* and two loss-of-function *Arabidopsis* mutants, *phb3* and *phb6*. For example, in the *Col-0* genetic background, synthetic peptides of PHB6 and PHB3 were used as competitive inhibitors at a ratio of 10:1 with the corresponding antibodies. Furthermore, the anti-PHB3 antibody was tested on both *Col-0* and *phb3*. Sections of both genotypes were incubated with anti-PHB3 antibody conjugated with Alexa Fluor 750 dye. The anti-PHB6 antibody specificity was examined on *Col-0* and *phb6* mutant. Sections of both genotypes were incubated with anti-PHB6 antibody and goat antirabbit IgG (H+L) labeled with Alexa Fluor 647 sequentially.

Super-Resolution Imaging

Super-resolution images were obtained using a home-built direct stochastic optical reconstruction microscopy (dSTORM) system with two excitation–emission channels based on a Nikon Ti-E inverted microscope.[90] A 656.5 nm diode-pumped

DOI: 10.1021/acs.jproteome.8b00320
J. Proteome Res. 2018, 17, 3195–3213

solid-state (DPSS) laser and a 750 nm diode laser were used for excitation of samples immune-labeled with Alexa Fluor 647 and Alexa Fluor 750 in imaging buffer.[90] A 100× objective lens (CFI Apo TIRFM 100× oil, N.A. 1.49, Nikon) was used to observe the fluorescence signals. An electron-multiplying charge-coupled device (EMCCD, Andor, IXon-Ultra) was applied to collect the emission light that passed through a channel splitter. To block the excitation laser and the channel crosstalk, emission filters FF01-692/40-25 and FF01-794/32-25 were used for the 647 and 750 nm channels, respectively. During imaging, the samples were stabilized using an active locking system with 1 nm accuracy. Static conventional fluorescence images using lower laser intensities (typically 89 W/cm^2 for 647 nm and 434 W/cm^2 for 750 nm) were obtained before super-resolution imaging to locate the target cells. The excitation laser intensities were 4.0 and 4.5 kW/cm^2 for Alexa Fluor 647 and Alexa Fluor 750, respectively. Every super-resolution image was accumulated by 10 000 frames at 33 Hz to record the blinking of fluorescent dye molecules with 200× the electron-multiplying (EM) gain. According to the average fitting error, 20 nm lateral resolution was achieved. The 3D images with 50 nm axial resolution were generated by applying a cylindrical lens. Rohdea 2.0 software (Nanobioimaging, Hong Kong) was used to process the data, and ImageJ software was used to reconstruct the final images.

Colocalization Analysis of Interacting Proteins Based on dSTORM Micrographs

Colocalization is a concept to describe the degree of interaction and relationship between two proteins. The two-color dSTORM system provides 3D super-resolution images with 50 axial resolution and 500 nm thickness. To calculate the 3D colocalization, the super-resolution image is divided into 10 layers, from −250 to 250 nm along the Z direction with 50 nm thickness. In the colocalization experiment analysis, a modified Manders split coefficient[91] was applied to calculate the colocalization for each layer and then to obtain the 3D colocalization. The Manders method is widely used to calculate colocalization. In this case, two colocalization coefficients are used to describe the degree of two molecules' overlapping[91]

$$M_1 = \frac{\sum_i R_{i,\mathrm{colocal}}}{\sum_i R_i}$$

$$M_2 = \frac{\sum_i G_{i,\mathrm{colocal}}}{\sum_i G_i}$$

where R and G are the intensity of the red channel (647 nm) and green channel (750 nm). $R_{i,\mathrm{colocal}} = R_i$ if $G_i > 0$, and $G_{i,\mathrm{colocal}} = G_i$ if $R_i > 0$. Coefficients M1 and M2 can range from 0 to 1. M1 = 1 implies that all of the pixels of the red components are located in pixels of the green components, while M2 = 1 implies that all pixels of the green components are located in pixels of the red components.

Additionally, if two images are merged together, another coefficient, r_{merge}, is proposed to calculate the ratio of the total intensity of overlapped pixels over two channels

$$r_{\mathrm{merge}} = \frac{\sum_i R_{i,\mathrm{colocal}} + \sum_i G_{i,\mathrm{colocal}}}{\sum_i R_i + \sum_i G_i}$$

The coefficient r_{merge} ranges from 0 to 1. $r_{\mathrm{merge}} = 1$ implies that the two channels are 100% colocalized.

Measurement of Rosette Area and Root Length of *Arabidopsis*

Photos of 38 day old plants were captured. In these photos, rulers are used to indicate the scale. The rosette areas were measured using ImageJ software with a downloaded module (http://dev.mri.cnrs.fr/projects/imagej-macros/wiki/Measure_Rosette_Area_Tool). The roots were gently separated from the medium, and their lengths were measured directly using a ruler. In a single biological replicate, typically 15−20 plant individuals of a genotype were assessed. A total of three biological experiments were performed.

Statistical Analysis

The statistical significances of plant phenotypes and immunoblotting were determined using the two-tailed Student's t test or one-sample t test. The significance values are represented by "*", "**", and "***" to indicate $P < 0.05$, $P < 0.01$, and $P < 0.001$, respectively. Multiple comparisons were assessed by one-way ANOVA (analysis of variance) using the IBM SPSS statistical package (version 24, IBM, Armonk, NY). The Tukey's range test of 5% significance was used.

RESULTS

Establishing Chemical Labeling, Chromatographic Enrichment, and Mass Spectrometry Analysis for IPQCX−MS

To identify protein−protein interactions in *Arabidopsis*, a comprehensive interactomics of five major steps was adopted (Figure 1A and Figure S6A): (1) in vivo chemical cross-linking with a specially designed cross-linker (Figure S6B), (2) CsCl density gradient (CDG) centrifugation-based fractionation of proteins and subsequent peptide preparation, (3) light- and heavy-isotope-coded dimethyl labeling and mixing of peptides, (4) SCX chromatography-based separation and affinity bead enrichment of the cross-linked peptides, and (5) LC−MS/MS analysis. According to this workflow (Figure 1A), both protein samples of the control and treated plant were extracted and subjected to CsCl density gradient centrifugation, which produced top (t), middle (m), and bottom (b) fractions with a yield (the ratio of protein amount to the tissue amount used for protein extraction) of 0.20%, 0.60%, and 0.07%, respectively. As a result, each biological replicate produced six protein samples (i.e., the control and treated ×3 CDG fractions, Figure 1A and Figure S6A). These proteins were digested into peptides with a yield (the ratio of peptide amount to protein amount) of 65−75%. After dimethyl labeling and peptide mixing, each biological replicate produced six mixing replicates (i.e., tF, mF, bF, tR, mR and bR; Figure 1A,B and Figure S6A).

To enrich the cross-linked peptides from the cellular peptides, the azido on the cross-linker was conjugated to the alkyne moiety of the disulfide bond-linked biotin and alkyne (DLBA) through click chemistry (Figure 1C). Following the click reaction, we further separated each peptide sample into three fractions using SCX-HPLC (Figure 1A). Finally, a single biological replicate generated 18 peptide mixtures (3 CsCl density gradient fractions × 2 types of mixing [F and R] × 3 SCX-HPLC fractions). In total, three biological replicates produced 54 peptide mixtures (18 peptide samples × 3 biological replicates). The biotin-tagged cross-linked peptides were subsequently enriched from each of 54 peptide samples via streptavidin affinity purification. Following a series of subsequent chemical modifications (Figure 1C), the cross-linked peptides were obtained with a yield of 0.13% to 0.22%. (The yield was defined to be a ratio of

DOI: 10.1021/acs.jproteome.8b00320
J. Proteome Res. 2018, 17, 3195−3213

the cross-linked peptide amount to the total amount of cellular peptides in each SCX-HPLC fraction.) The enriched cross-linked peptides were finally subjected to LC−MS/MS analysis, which has thus far completed the first two C steps of IPQCX−MS (Figure 1A and Figure S6A). To facilitate the computational analysis of the mass spectrometry (MS/MS) data, 18 MS data sets prepared from a single biological replicate were combined into two larger MS/MS data sets separately (F and R, Figure S6A).

Identification and Quantitation of in Planta Cross-Linked Peptides

To confirm if the in vivo cross-linking was successful, AMDSP monolinked (dead-end) peptides were identified and measured with a cutoff FDR threshold of ≤ 0.01. Altogether, we found 11 820 unique monolinked peptides (Table S2b) from 77 226 redundant monolinked peptides (Table S2a). Cellular components analysis results suggested that these peptides are from cellular proteins inside the cell rather than secretary proteome (Table S2c), which confirmed that AMDSP had been successfully delivered into plant cells through vacuum infiltration.

To establish a comprehensive and multitask computational program for identifying and quantifying light- and heavy-isotope-labeled cross-linked peptides, we coupled a modified SQUA-D (version 2.0)[77] with ECL2 (version 2.1.7).[45] ECL2 can search all possible peptide−peptide pairs through an exhaustive approach, while other state-of-the-art tools, such as xQuest, pLink, and Kojak, only search a small fraction of all peptide−peptide pairs for each spectrum with prefiltering steps. Such prefiltering steps may cause missed findings.[44,45] The XIC-based quantification component, SQUA-D, uses the output of the cross-linked peptide identification as an input to locate the ion chromatography profile for each identified PSM (Figure 2). The new version of SQUA-D estimates the intensities and calculates the log-ratio of light- and heavy-isotope-labeled PSMs. Finally, it outputs the log ratios of all identified PSMs and supplies the consequent results to a statistical evaluation component (Figure 2). The statistical evaluation component includes the batch effect adjustment,[92] *t* test, and multiple test correction.[93] All of these components are illustrated in the workflow (Figure 2).

Because ECL2 included contaminant proteins during the searching automatically, we eliminated the PSMs belonging to those contaminants in the downstream analysis. Furthermore, because our samples were labeled with light or heavy dimethyl labeling, we eliminated the PSMs without the labeling or containing the incorrect labeling patterns. With FDR ≤ 0.05, a total of 3171 PSMs (Table S3a) were identified. These PSMs contained 354 unique cross-linked peptides (Table S3b). We also include a table (Table S3c) containing PSMs with FDR ≤ 0.01.

We also analyzed our data with pLink (version 2.3.3) and Kojak (version 1.5.5). The same parameters and selection criteria were used. For the interprotein cross-linked peptides, pLink identified 2 PSMs, Kojak identified 0 PSMs, and ECL2 identified 92 PSMs (Figure S4A). For the intraprotein cross-linked peptides, pLink identified 3 PSMs, Kojak identified 3047 PSMs, and ECL2 identified 3079 PSMs (Figure S4B). Both pLink and Kojak did not identify many interprotein cross-linked peptides, which may be caused by their prefiltering steps. These steps compare spectra with linear peptide chains and discard low confident peptide chains before generating peptide−peptide pairs and scoring. Although such steps are reasonable to some extent, it may cause missed findings when the database is large.[44,45] In terms of average running time for analyzing one data file, pLink took 1.17 h, Kojak took 0.95 h, and ECL2 took 2.4 h. Kojak and ECL2 were run in a Linux server with two Intel Xeon E5-2670 v3 CPUs (12-core, 2.3 GHz) and 64 GB RAM. pLink was run in a Windows PC with one Intel Xeon E5-2630 v4 CPU (10-core, 2.2 GHz) and 64 GB RAM. Please refer to the Supplemental File for the parameter files, the log files, and the results.

Among the unique cross-linked peptides identified by ECL2, 241 and 271 cross-linked peptides were light- and heavy-isotope-labeled, respectively (Table S3b, Figure 3A). After combining the three CsCl fraction peptide mixing types, tF1, mF1, and bF1, into a single F1 experiment replicate sample, we found that the number of unique cross-linked peptides accumulated as the number of experimental replicates increased (Figure 3B). Altogether, 21.19% of the 354 unique cross-linked peptides were identified 10 times or more, and 41.53% of them were identified once (Figure 3C). The charges of 53.28% of the unique cross-linked peptides were +4 (Figure 3D). Using the leaf proteome of *Arabidopsis* as a reference,[85] we defined those proteins having spectral counts ≥ 100 as abundant proteins. As a result, we found, notably, that 38.60% of the unique cross-linked peptides (i.e., PSM number ≥ 1), 40.32% of those identified at least twice among the unique cross-linked peptides (i.e., PSM number ≥ 2), and 41.30% of those identified at least four times among the unique cross-linked peptides (i.e., PSM number ≥ 4) were actually from the abundant proteins in our experiments, and their ratios were much larger than the ratio of abundant proteins in leaf the proteome of *Arabidopsis* (i.e., 9.12%, Figure 3E). This finding strongly suggests that the interactions of abundant proteins are preferable for capture by IPQCX−MS-based interactomics.

GO analysis of those proteins derived from the cross-linked peptides showed that the in vivo cross-linked proteins were concentrated in the following categories, molecular function 1−3, biological process 7−9, and cellular component 13−15, and were reduced in the following categories, molecular function 4−6, biological process 10−12, and cellular component 16−18 (Figure 3F and Figure S7). These findings suggest that IPQCX−MS-based interactomics tends to capture the proteins located in the cell wall, extracellular space, and cytoplasm rather than those located in the nucleus. In addition, stable interactions, such as interactions between structural molecules, are preferable to be captured instead of transient interactions, such as interactions between signal transduction molecules (Figure 3F and Figure S7).

Among the 354 unique cross-linked peptides identified, there are 61 interprotein cross-linked peptides and 293 intraprotein cross-linked peptides (Table S3b). The cross-linked peptide $_{205/205/203}$AKFIVEK(α)−$_{187}$AVEQKQVAQQEAER(β) is one of those interprotein cross-linked peptides found (Table S3b). Its α and β chains were derived from prohibitin 1/2/6 (PHB1/PHB2/PHB6, AT4G28510/AT1G03860/AT2G20530) and PHB3 (AT5G40770), respectively. Its MS/MS spectra of heavy isotope-labeled cross-linked peptides are shown in Figure 3G. Three D structure models and docking of PHB3 and PHB6 are predicted as shown in Figure 3H. The predicted distance between the two cross-linked lysines (i.e., PHB3-K191 and PHB6-K204) was 18.1 Å according to the model (Figure 3I).

Among the 61 interprotein cross-linked peptides, seven interactions were found in the STRING database, and they are $_{205/205/203}$AK**F**IVEK−$_{187}$AVEQ**K**QVAQQEAER of the PHB1/PHB2/PHB6 and PHB3 interaction, $_{37}$KTVA**K**PK−$_{49}$S**K**AVSETSDELAK of the light-harvesting chlorophyll A/B-binding protein 1.1 (LHCB1.1, AT1G29920) and LHCB5 (AT4G10340) interaction, $_{37}$KTVA**K**PK−FFDPLGLAADPE**K**TAQLQLAEIK

DOI: 10.1021/acs.jproteome.8b00320
J. Proteome Res. 2018, 17, 3195−3213

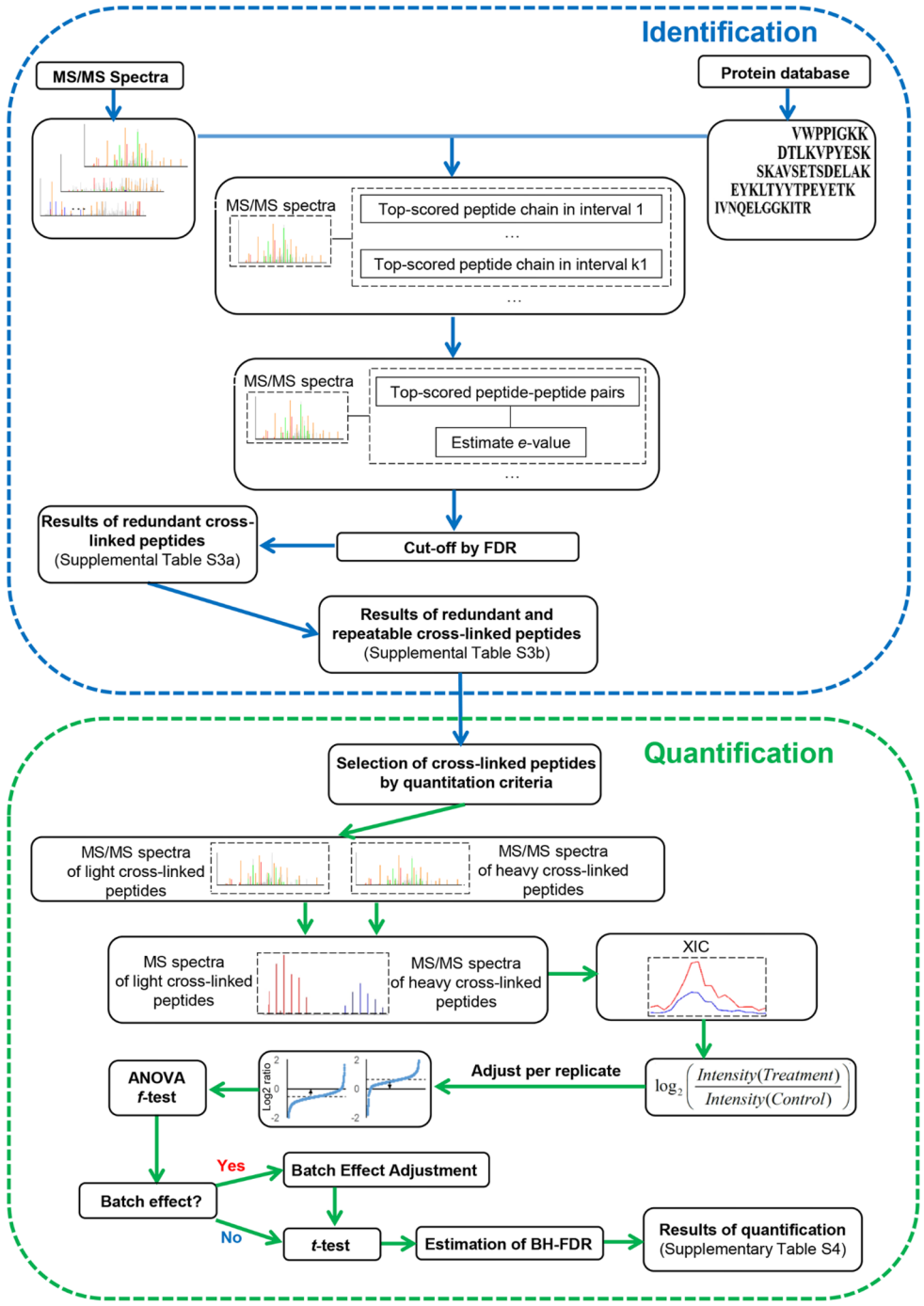

Figure 2. Flowchart of the computational programs of ECL2 coupled to a quantification module. Cross-linked peptides were evaluated based on FDR ≤ 0.05, where FDR is the false discovery rate estimated based on the target-decoy. The identification component is provided in Table S3a,b, whereas the quantification was performed according to the XIC of cross-linked peptides. The calculation of XIC log-ratios was followed by a statistical evaluation procedure that included both the *t* test and multiple test correction (i.e., BH-FDR). The significant cutoff criteria were BH-FDR ≤ 0.1 and $|\text{log-ratio}| \geq 0.58$ (i.e., $|\text{fold change}| \geq 1.5$). The quantification component outputs are provided in Table S4.

of the LHCB1.1 (AT1G29920) and LHCB4.1 (AT5G01530) interaction, $_{375}$**K**YGSGGA−$_{176}$IINEPTAAAIAYGLD**K**K of the ADP/ATP carrier 1 (AAC1, AT3G08580) and heat shock protein 70-1 (HSP70-1, AT5G02500) interaction, $_{2}$AST-SLLK−$_{176}$LTGTDVGYPGGLWFDPLGWGSGSPA**K**LK of the fructose-bisphosphate aldolase 2 (FBA2, AT4G38970) and photosystem I light-harvesting complex gene 2 (LHCA2, AT3G61470) interaction, $_{377}$VGSAAQL**K**AMK−$_{467}$TNKPQF-QEIIAST**K**TLTAEAESFLK of the ATPase subunit 1 (ATP1, ATMG01190) and ATPase subunit alpha (ATPA, ATCG00120) interaction, and $_{98}$SGGAGASE**K**K−$_{621}$GSQGAVT**K**DK of the ribosomal protein L36e family protein (AT5G02450) and SRP72 RNA-binding domain-containing protein (AT1G67680) interaction. This alternative evidence supports the results of the IPQCX−MS approach.

During the quantitation of cross-linked peptides, the batch effect adjustment (Figure 2) was applied to 18 replicates of the MS data sets (generated from 3 biological replicates × 2 types of

DOI: 10.1021/acs.jproteome.8b00320
J. Proteome Res. 2018, 17, 3195−3213

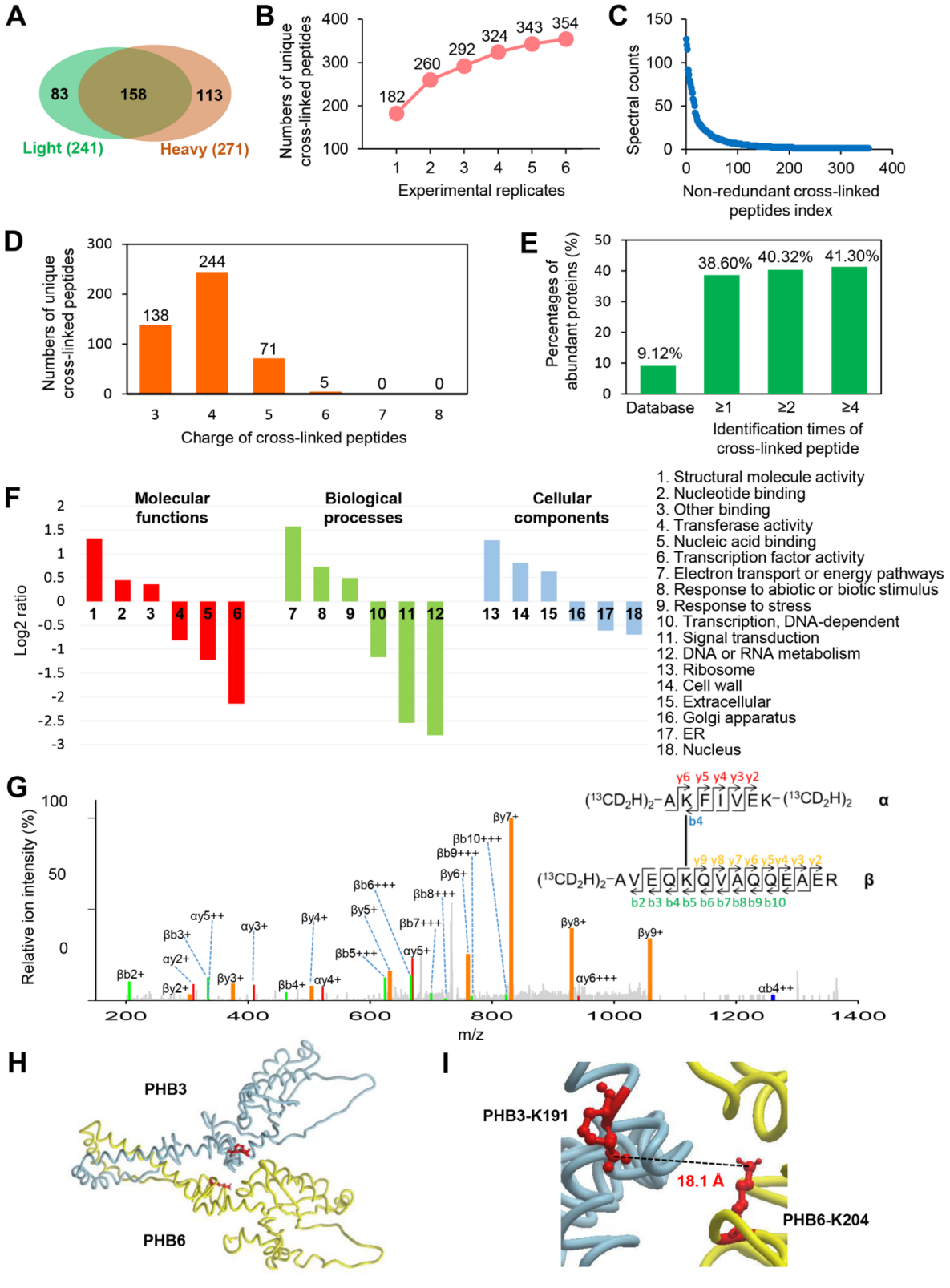

Figure 3. Mass spectrometry and bioinformatics analysis of cross-linked peptides. (A) Venn diagram presentation of the identified unique light- and heavy-isotope-labeled cross-linked peptides. (B) Accumulation of the identified unique cross-linked peptides from six experimental replicates. (C) Relationship between the spectral count and the index of unique cross-linked peptides. (D) Charge distribution of unique cross-linked peptides. The charge range for identification ranged from +3 to +8. (E) Percentages of abundant proteins in the leaf proteome of *Arabidopsis* and cross-linked proteins from the cross-linked peptides with different identification times. (F) Comparison of the GO analysis results between the cross-linked proteins and the leaf proteome of *Arabidopsis*. Protein categories of the highest and lowest three log-ratios are shown. (G) MS/MS spectra of interprotein cross-linked peptide AKFIVEK-AVEQKQVAQQEAER between PHB3 (Prohibitin 3, AT5G40770) and PHB6 (AT2G20530) proteins. (H) 3D structure of the protein−protein interaction between PHB3 and PHB6. (I) Magnified view of the cross-linked sites between PHB3-K191 and PHB6-K204.

DOI: 10.1021/acs.jproteome.8b00320
J. Proteome Res. 2018, 17, 3195−3213

mixings × 3 CsCl protein fractions, Figure 1A and Figure S6A). This batch effect adjustment aims to fine-tune the corresponding technical and experimental errors resulting from treatment, the CDG centrifugation fractionation of proteins, and the peptide digestion as well as the chemical labeling/mixing.[77] According to the criteria mentioned in the Experimental Section, 86 L- and H-labeled cross-linked peptide pairs were selected for quantification (Table S4). The criteria for selecting the cross-linked peptides for quantitation analysis are defined as follows: |fold change| ≥ 1.5 (or |log-ratio| ≥ 0.58) and multiple-testing-corrected FDR (BH-FDR[94]) ≤ 0.1. Nine and three cross-linked peptides were found to be hormone-enhanced and -suppressed, respectively (Figure 4A and Table S4). For example, the intraprotein cross-linked peptide $_{188}$**K**PEVEEK−$_{175}$**K**GETPETAVVEEK derived from the plasma-membrane-associated cation-binding protein 1 (PCAP1, AT5G38410) changed 4.94-fold in response to ethylene hormone treatment (Figure 4B and Table S4), while the intraprotein cross-linked peptide $_{201}$VQTSSGE**K**PVR−$_{212}$ELV**K**DDAWLDGEFISTVQQR derived from cytosolic-NAD-dependent malate dehydrogenase 1 (C-NAD-MDH1, AT1G04410) had a −2.41-fold change (the negative sign corresponds to down-regulation) due to the ethylene hormone treatment (Figure 4C and Table S4). The ethylene production rate of the ACC-treated plants is much higher than that of the control (Figure S8A). We also found that ethylene treatment induced a smaller rosette area and shorter root length in both the wild-type *Arabidopsis Col-0* and *ein3/eil1* mutant (Figure S8B,C). These hormone-regulated cross-linked peptides, reflecting possible ethylene-regulated protein−protein interactions and protein conformation changes, may participate in ethylene-regulated plant growth.

Confirmation and Validation of Interaction of PHB3 and PHB6 with Alternative Method

To confirm the protein−protein interaction and conformation changes instantly captured in vivo, we have designed alternative biochemical and microscopic methods. The cross-linked peptide derived from the interaction of PHB6 and PHB3 was chosen for this validation. To that end, anti-PHB3 and anti-PHB6 antibodies were generated (see the Experimental Section). To test the specificities of anti-PHB3 and anti-PHB6 antibodies, immunoblotting was performed on *Col-0* and the loss-of-function *Arabidopsis* mutants *phb3* and *phb6* (Figures S5 and S9B,C). As compared with *Col-0*, the *phb3* mutant still retained a background of weak immune-reactivity signal (i.e., 29.87% of the full signal) using anti-PHB3 antibody because of the similarity of the primary amino acid sequences among PHB3, PHB4, and PHB5 (Figure S9A). We found that the protein level of PHB3 was ethylene hormone-suppressed in the genotypes of *Col-0*, *ein3/eil1*, and *phb6* (Figure S9B,D), whereas the background signal generated by the anti-PHB3 antibody in the *phb3* mutant was not ethylene-regulated (Figure S9B). Similarly, when the anti-PHB6 antibody was employed, immunoblotting was performed on both the *Col-0* and *phb6* mutant. These results show that the PHB6 protein missed the immunoreactivity signal in the *phb6* mutant background (Figure S9C), suggesting the specificity of the anti-PHB6 antibody, and, interestingly, the protein level of PHB6 was ethylene hormone-enhanced in both the *Col-0* and *ein3/eil1* genetic backgrounds (Figure S9C,E).

Given the specificity of the anti-PHB3 and anti-PHB6 antibodies, we adopted the coimmunoprecipitation approach to confirm the results of IPQCX−MS. The corresponding preserums of the anti-PHB3 antibody and anti-PHB6 antibody

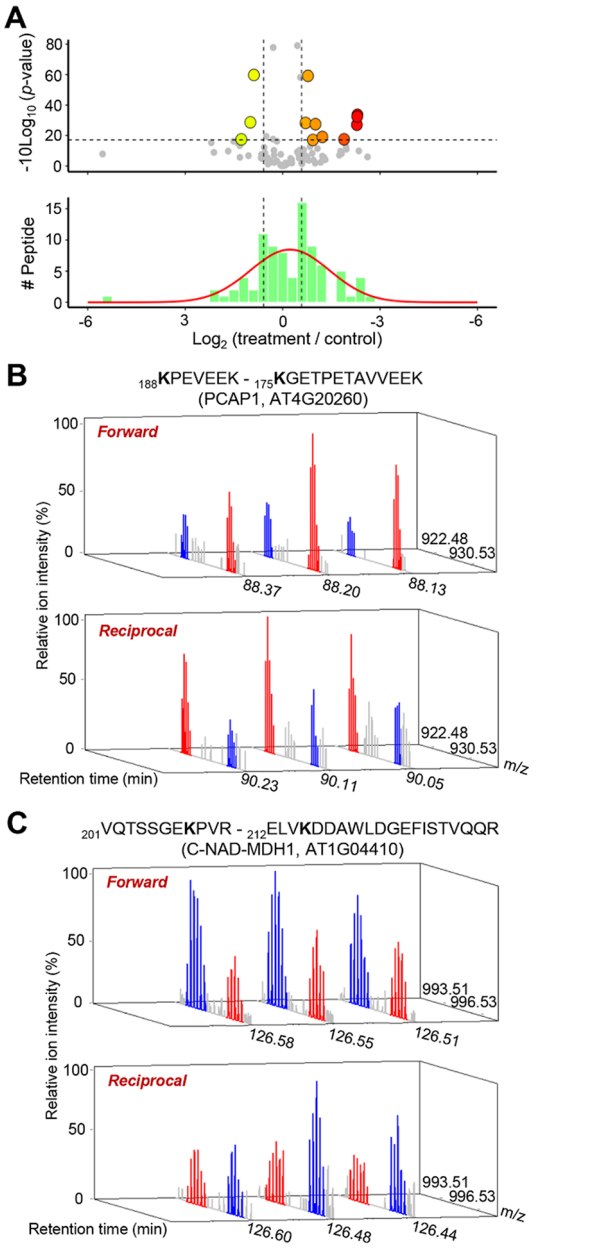

Figure 4. Quantitative interactomics in *Arabidopsis*. (A) Circles in the upper panel designate the quantified cross-linked peptides, while the red and yellow circles are hormone-enhanced and hormone-suppressed cross-linked peptides, respectively. The *x* axis shows the average log-ratios from pairs of treatment and control ions. The *y* axis is the value of −10 times the log-transformed *p* value. *BH − FDR* ≤ 0.1 was used as the significance cutoff threshold. The corresponding *p*-value threshold is indicated by the horizontal dashed line. The boundaries of |log-ratio| ≥ 0.58 (i.e., |fold change| ≥ 1.5) are shown by two vertical dashed lines. A histogram (green) and a fitted Gaussian distribution (red) of all quantified cross-linked peptides are shown in the lower panel. The *x* axis shows the average log-ratio, and the *y* axis indicates the number of cross-linked peptides in the corresponding histogram bin. The boundaries of |log-ratio| ≥ 0.58 (i.e., |fold change| ≥ 1.5) are shown by two vertical dashed lines. (B) Mass spectra of the light- and heavy-isotope-labeled hormone-enhanced and intraprotein cross-linked peptide KPEVEEK-KGETPETAVVEEK from plasma-membrane-associated cation-binding protein 1 (PCAP1, AT5G38410). (C) Mass spectra of the light- and heavy-isotope-labeled hormone-suppressed and intraprotein cross-linked peptide VQTSSGEKPVR-ELVKDDAWL-DGEFISTVQQR from cytosolic-NAD-dependent malate dehydrogenase 1 (C-NAD-MDH1, AT1G04410).

DOI: 10.1021/acs.jproteome.8b00320
J. Proteome Res. 2018, 17, 3195−3213

were applied as a negative control. To ensure that the same amount of IgG was used for the antibodies and the preserums, calibration was performed according to immunoblot analysis (Figure S10A,B). The anti-PHB3 antibody was able to pull down both PHB3 and PHB6, whereas the anti-PHB6 antibody was able to pull down both PHB6 and PHB3 reciprocally (Figure 5A). A smaller protein band could be visualized in the input when it was set against the anti-PHB3 antibody, which may represent a segment of the PHB3 protein (Figure 5A). This possible partial PHB3 protein did not come from in vitro artificial proteolytic degradation because it could be detected in both the input and flow-through of similar percentages (Figure S10C). It is likely that the segment of PHB3 protein was more easily enriched by coimmunoprecipitation using the PHB6 antibody (Figure 5A). The coimmunoprecipitation experiment strongly suggests that the PHB3 protein interacts with PHB6 in plant cells, as shown in the IPQCX−MS analysis.

The interaction between PHB3 and PHB6 protein was also examined by mass shift assay. To do this, the plants were separated into two groups: One was infiltrated with 1% formaldehyde in the cross-linking buffer, while the other group had the cross-linking buffer only as a control. After the cross-linking reaction, both PHB3 and PHB6 proteins were shifted to ∼63 kDa on SDS-PAGE according to the protein size markers (Figure 5B). Because the size of PHB3 and PHB6 was determined to be 30.4 and 31.6 kDa, respectively, according to bioinformatics, the 63 kDa size of the PHB3 and PHB6 protein detected on SDS-PAGE suggested that they were successfully cross-linked under formaldehyde treatment (Figure 5B).

To further validate the interaction between PHB3 and PHB6 proteins, the super-resolution imaging technique was also applied. To do this, 750 nm dye was conjugated to the anti-PHB3 antibody, while 647 nm dye was conjugated to goat antirabbit IgG antibody, which was used as a secondary antibody to recognize the primary anti-PHB6 antibody. Because the autofluorescence of plant cells could be observed in both channels by conventional fluorescence imaging (or called wide-field micrographs, Figures S11A and S12A), only dSTORM micrographs were used to verify the colocalization of PHB3 and PHB6 protein. The titration experiments (Figures S11C and S12C) and *phb3* and *phb6* loss-of-function mutant (lack of PHB3 or PHB6 protein) immunohistological experiments (Figures S11D and S12D) using the anti-PHB3 and anti-PHB6 antibodies revealed the specificities of these two antibodies in recognizing the target PHB3 and PHB6 proteins. Figure 5C and Figure S13A,C,E show the overlapping localization (yellow) of PHB3 (green) and PHB6 (red) inside cells. The colocalization results between PHB3 and plasma membrane intrinsic protein 2A (PIP2A, AT3G53420) (Figure S14A,C,E) as well as between PHB6 and PIP2A (Figure S15A,C,E) were used as negative controls. These two controls showed that both PHB3 and PHB6 were located far from the membrane-localized water channels.

Three 3D super-resolution images were obtained for each pair of proteins. Every 3D image was divided into 10 layers, from −250 to 250 nm, along the *Z* direction with a thickness of 50 nm. Colocalization coefficiencies of PHB3 versus PHB6, PHB3 versus PIP2a, and PHB6 versus PIP2a were calculated according to a statistical method (see Experimental Section, Figure 5D) based on the protein pairs found in a total of 30 layers of the super-resolution micrographs (Figures S13B,D,F, S14B,D,F, and S15B,D,F). The average colocalization coefficiency of the PHB3 versus PHB6 pair was 0.77, which was significantly larger than that of the PHB3 versus PIP2A and PHB6 versus PIP2A pairs (i.e., 0.14 and 0.31 colocalization coefficiency, respectively, Figure 5D). The larger colocalization coefficiency means the higher possibility of colocalization of the two proteins. Taken together, these alternative molecular and microscopic data confirmed the interaction of PHB3−PHB6 protein initially identified via the IPQCX−MS approach.

Measurement of Morphologies of *phb3* and *phb6* Mutants

To confirm that the in planta cross-linked PHB3−PHB6 protein complex plays a biological role in *Arabidopsis*, we measured the rosette area and root length of 38 day old wild-type *Col-0* and *phb6* and *phb3* mutant plants. In the case of the rosette area, *phb6* showed a 25.7% increase as compared with the wild type, whereas *phb3* showed a 24.5% reduction as compared with *Col-0* (Figure 5E). In contrast, the root of *phb3* exhibited a 65.5% reduction in length, whereas *phb6* remained unchanged as compared with *Col-0* (Figure 5E).

DISCUSSION

The IPQCX−MS has facilitated the identification of hundreds of unique in planta cross-linked peptides (Table S3b) from *Arabidopsis*. The identified cross-linked peptides provide new insights into in vivo protein conformation changes and protein−protein interaction dynamics simultaneously. In addition to size exclusion chromatography (SEC) and SCX-based chromatography,[17,22] a biotin−streptavidin affinity enrichment was applied in the experiment to highly enrich the cross-linked peptides.[24,28,95] On the basis of our multistep workflow, 0.13 to 0.22% cross-linked peptides were yielded from the total cellular peptides. TCEP was found to be efficient in eluting the cross-linked peptides off biotin−streptavidin resin. The removal of biotin from the cross-linker is believed to facilitate MS/MS analysis.[28]

The identification of 354 unique cross-linked peptides by a combination of both AMDSP-based cross-linking and ECL2 is comparable to the finding of 240 cross-linked peptides by the DSBSO-based cross-linking in HEK 293 cells,[28] even though it seems smaller than the 3323 cross-linked peptides identified by the PIR-containing cross-linker in HeLa cells.[22] One possible explanation for the difference is the multiple cellular structures and the more than 100 different amine-contained secondary metabolites present in plants,[32] which may titrate the penetrated AMDSP, impeding the in vivo cross-linking of proteins in higher plants. Another possible explanation may be the different lengths of cross-linker spacers. AMDSP-, DSBSO-, and PIR-containing cross-linker spacers are 9.6, ∼14,[28] and 43 Å[24] long, respectively. The application of various arm lengths of cross-linkers together in a single experiment was considered. However, because this hybrid cross-linker approach may raise the risk of computational analysis and divide the ion intensity of one cross-linked peptide into several, we therefore abandoned it. Moreover, the working concentrations of AMDSP-, DSBSO-, and PIR-containing cross-linkers applied in various experiments were 1, 2,[28] and 10 mM,[22] respectively. The relatively lower concentration of cross-linker used may result in fewer cross-linked peptides in our case.

Biological process and cellular component enrichment analysis were performed on 386 cross-linked proteins (corresponding to 354 cross-linked peptides) identified by AMDSP-based cross-linking, 56 cross-linked proteins identified by DSBSO-based cross-linking,[28] and 893 cross-linked proteins identified by PIR-containing cross-linkers.[22] AMDSP-based interactomics' results were concentrated in protein neddylation, the reductive pentose-phosphate cycle, and carbon utilization by fixation of carbon dioxide, whereas DSBSO- and PIR-containing

DOI: 10.1021/acs.jproteome.8b00320
J. Proteome Res. 2018, 17, 3195−3213

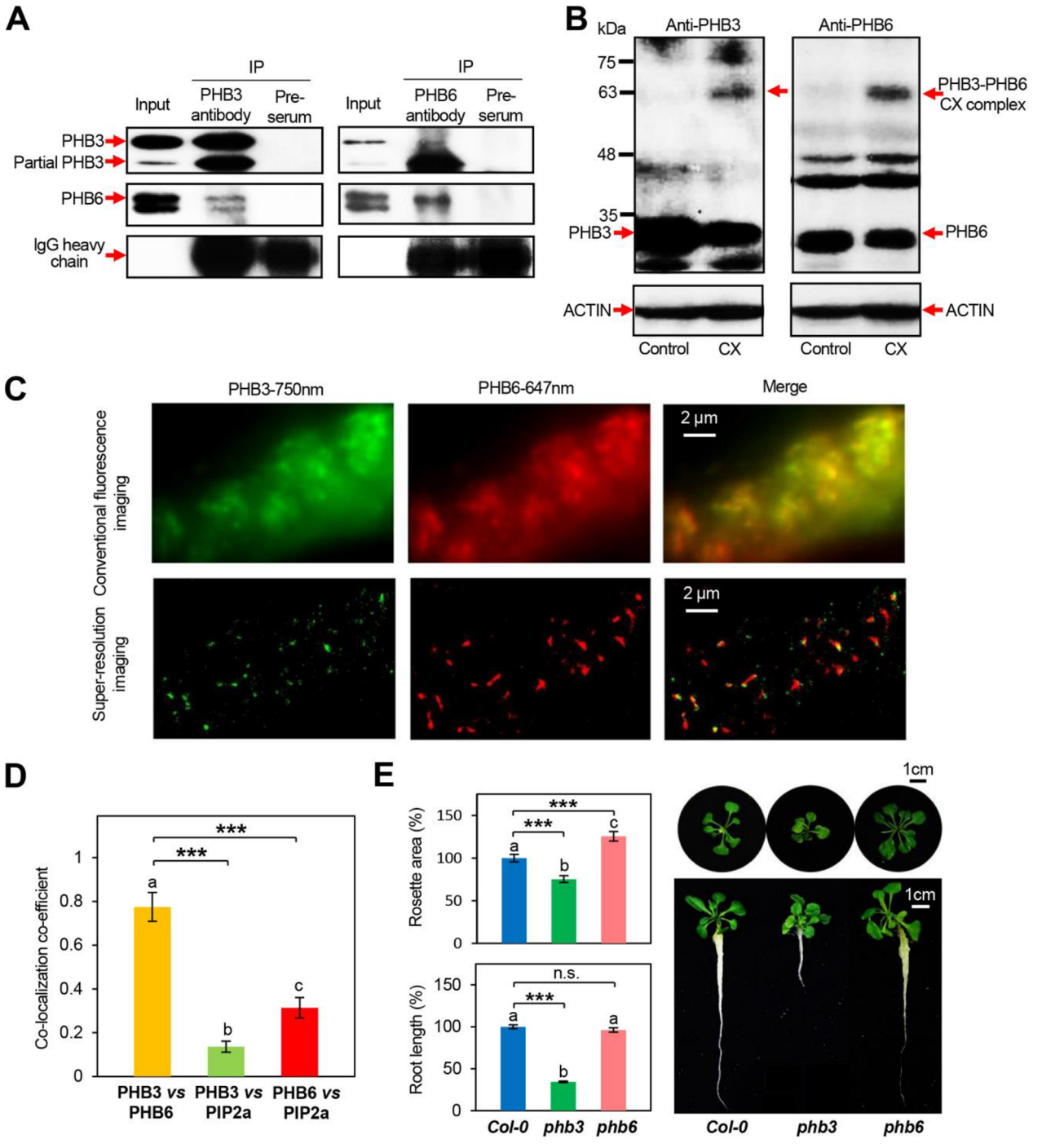

Figure 5. Confirmation of in planta PHB3 and PHB6 interaction and their functions during growth. (A) Coimmunoprecipitation of PHB3 and PHB6 in *Arabidopsis* crude extract. The crude extract (3%) was used as input. Precipitates of preserum (collected before immunoreaction) of each antibody were used as a negative control. The left panel shows the precipitates of anti-PHB3 antibody, and the right panel shows the precipitates of anti-PHB6 antibody. The presence of PHB3 and PHB6 were visualized by immunoblot analysis using antibodies against PHB3 and PHB6, respectively. (B) In vivo cross-linking (CX) of the PHB3−PHB6 complex by 1% formaldehyde. The left panel is against anti-PHB3 antibody, and the right panel is against anti-PHB6 antibody. Proteins extracted from the plants that went through infiltration in cross-linking buffer without cross-linker were used as a control. (C) Super-resolution imaging of PHB3 and PHB6. The upper three photos show wide-field fluorescence imaging, and the lower three photos show dSTORM super-resolution imaging. The left two photos show labeling with anti-PHB3 antibody with 750 nm dye. The middle two photos are labeled with anti-PHB6 antibody with 647 nm dye. The right two photos are merged images. (D) Colocalization coefficients of PHB3 versus PHB6, PHB3 versus PIP2a (plasma membrane intrinsic protein 2a, AT3G53420), and PHB6 versus PIP2a. Three photos of 3D dSTORM super-resolution imaging were collected for each pair of proteins. Every photo is divided into 10 layers, from −250 to 250 nm, along the *Z* direction with 50 nm thickness. There were 30 layers in total for one pair of proteins. The colocalization coefficient of each layer was calculated. Average values and error bars (±SEM) are shown. ANOVA and *t* test were used to evaluate significant differences. (E) Measurement of the *Arabidopsis* rosette area and root length. Three biological replicates were assessed. Average values and error bars (±SEM) are shown. The total plant numbers for every genotype to measure the rosette area were 54 for *Col-0*, 57 for *phb3*, and 55 for *phb6*. The total plant numbers for every genotype to measure root length were 55 for *Col-0*, 60 for *phb3*, and 60 for *phb6*. One-way ANOVA and *t* test were used to evaluate significant differences.

DOI: 10.1021/acs.jproteome.8b00320
J. Proteome Res. 2018, 17, 3195−3213

cross-linker-based interactomics's results were enriched in nucleosome assembly, chromatin assembly, and protein−DNA complex assembly in addition to ribosomal large subunit biogenesis, ribosomal small subunit biogenesis, and translational elongation (Table S5). Furthermore, the cellular component enrichment analysis of three cross-linker-identified proteins indicated that AMDSP-dependent interactomics showed an enrichment in the light-harvesting complex, mitochondrial envelope, and photosystem I, whereas DSBSO and PIR cross-linkers were enriched in the nucleosome, protein−DNA complex, and chromatin in addition to the chaperonin-containing T-complex, proteasome core complex, alpha-subunit complex, and the eukaryotic translation initiation factor 3 complex eIF3m (Table S5). These results suggest that the three different cross-linking strategies were enriched for different biological processes and cellular components. Thus they may be complementary to each other in the discovery of various interactomes of plants.

As both the DSBSO cross-linker[28] and PIR-linkers[24] used for in vivo cross-linking are MS-cleavable, this class of cross-linkers used in the identification of cross-linked peptides relies on the MS^3 spectra. More cycling time must be used to generate MS^3 spectra, which may reduce the number of MS^2 spectra and result in reduced identification.[96] As compared with the number observed using the MS^2 spectra-based identification, there is an overall 18% reduction in the number of total redundant peptides and a 13% reduction in the number of nonredundant peptides using MS^3 spectra.[97] In our case, we adopted an approach to combine the in vivo chemical cross-linking with the identification of cross-linked peptides using MS^2 spectra assisted by ECL2 software. It is likely that the application of both MS-cleavable and MS-noncleavable approaches in a single cross-linking experiment may help identify a greater number of cross-linked peptides.

In contrast with other cross-linked peptide identification tools,[40,42,43,53] ECL2 searches all possible peptide−peptide pairs so that missed findings can be avoided. We have used various data sets to demonstrate that ∼30% of the findings are missed.[44,45] Most importantly, this missed-finding issue is exacerbated for larger databases. ECL2 also performs exhaustive searching of all peptide−peptide pairs with a linear time complexity. With such a strategy, it can identify cross-linked peptides by searching all possible peptide−peptide pairs from a larger database (e.g., 5538 proteins) within a few hours.

The previous transgenic plant approach and affinity-tag-based enrichment have demonstrated that PHB1/2/3/4/6 can be copurified with PHB3[98] and PHB1.[99] In the present study, we have confirmed the interaction of PHB3 and PHB6 by in vivo chemical cross-linking (Table S3b and Figure 3H), which is considered to occur under native cytoplasmic conditions. The unique interaction between PHB3 and PHB6 is confirmed using alternative biochemical methods and super-resolution imaging. We also provided structural information about the interaction because the arm length of the AMDSP cross-linker is well known. It has been reported that prohibitin proteins are ubiquitous, highly conserved, and primarily located on the inner mitochondrial membrane, although they have additional mitochondrial functions[100] and they are involved in the biological processes of *m*-AAA protease-associated protein degradation, assembly of OXPHOS complexes, mitochondrial DNA organization, cristae morphogenesis, ROS formation, protein and lipid scaffolds, and cellular proliferation and tumor repression.[99,101] The type-I PHB−type-II PHB heterodimer can assemble into a ring-shaped supercomplex in yeast[102] and *Arabidopsis*.[103] In addition to being parts of a complex, both type-I and type-II PHB proteins can also function independently.[98,104] In *Arabidopsis*, PHB3, PHB4, and PHB5 belong to type-I PHB, whereas PHB1, PHB2, PHB6, and PHB7 belong to type-II PHB.[105] Our findings suggest that type-I representative PHB3 and type-II representative PHB6 interact with each other under native conditions (Figures 3H and 5). Mutation of *phb3* leads to growth retardation of both the shoot and root,[98] which is consistent with our observations (Figure 5E). Double mutants *phb2/phb6* have a reduced rosette diameter.[99] In contrast with previous findings showing that *phb6* has a similar rosette diameter to the wild type[99] (Figure S16), we found that the rosette area of 38 day old *phb6* was larger than that of *Col-0* when grown in MS medium (Figure 5E), which suggests that the mechanism underlying the role of PHB6 in plant development is complex. A previous report concluded that PHB3 is involved in the ethylene signaling pathway.[106] Using an immunoblot analysis, we found that the PHB3 protein level was ethylene-suppressed (Figure S9D), while the PHB6 protein level was ethylene-enhanced (Figure S9E) instead in both *Col-0* and *ein3/eil1* backgrounds. How PHB complexes regulate ethylene response remains to be elucidated.

The in vitro isotopic dimethyl-labeling-based quantitation in combination with in vivo cross-linking is not only applicable in the medium-grown model plant *Arabidopsis*. This approach can also be applied in various field-grown crops. MS/MS-based quantification (e.g., iTRAQ and TMT labeling) and label-free-based quantification have the same application capability as dimethyl labeling. The MS/MS mass-spectrogram-based quantification measures a limited number of mass spectra,[58] and the label-free quantification depends on highly consistent sample preparation and analysis.[59,75] In contrast, the dimethyl labeling approach is reliable, quick, and cost-effective, with fewer side reactions and high labeling efficiency.[58,59] Both ratio adjustment of light and heavy ion intensity and batch effect adjustment reduce the statistical bias introduced by multiple experimental steps.[77]

The IPQCX−MS analysis revealed that all 12 ethylene-regulated cross-linked peptides resulted from intraprotein cross-linking events (Table S4). An ethylene-enhanced cross-linked peptide, $_{166/132/132}$KYYEAGAR−$_{59/25/25}$GILAADESTGTIGKR, may be derived from a likely interprotein cross-linking event among fructose-bisphosphate aldolase isoforms 4, 6, and 8 (or called FBA4/6/8) (Table S4). This probable interaction between FBA4 (AT5G03690) and FBA8 (AT3G52930) is supported by the protein−protein interaction data deposited in the *Arabidopsis* Interactions Viewer database.[107] We are currently unable to differentiate whether it is the interprotein or the intraprotein cross-linking occurring among these FBA protein isoforms that shares homologous amino acid sequences.

The ethylene hormone-regulated isotopic cross-linked peptides possibly result from one of two situations. The first possibility is that ethylene alters the gene expression of ethylene-responsive proteins, and the interaction of either increased or decreased ethylene-responsive proteins may contribute to the change of the cross-linked peptides' levels. The second possibility is that ethylene alters the protein conformation via ethylene-regulated post-translational modifications (PTMs), which further generate hormone-regulated intraprotein and interprotein cross-linked peptides. To differentiate these two possibilities, we have quantified some of the total cellular peptides (non-cross-linked linear peptides) and found that some ethylene-regulated linear peptides share the same protein origins as ethylene-regulated cross-linked peptides (Table S6a). For

DOI: 10.1021/acs.jproteome.8b00320
J. Proteome Res. 2018, 17, 3195−3213

example, the cross-linked peptide $_{132}$KYYEAGAR−$_{25}$GILAADESTGTIGKR derived from FBA4/6/8 isoforms had a 1.63-fold (>1.5-fold) increase, whereas the linear peptide $_{149}$IGENEPSEHSIHENAYGLAR derived from the same protein group had a 2.23-fold increase (>1.5-fold) upon ethylene treatment (Table S6b), which suggests that the up-regulation of this cross-linked peptide probably resulted from an increase in protein level. Moreover, both cross-linked peptides, $_{205}$AASFNIIPSSTGAAKAVGK−$_{123}$VVISAPSKDAPMFVVGVNEHEYK and $_{205}$AASFNIIPSSTGAAKAVGK−$_{123}$VVISAPSKDAPM(oxidation)FVVGVNEHEYK, derived from glyceraldehyde-3-phosphate dehydrogenase C subunit 1 (GAPC1, AT3G04120) were insignificantly altered to −1.23- and −1.22-fold, respectively. However, their corresponding linear peptides, $_{205}$AASFNIIPSSTGAAK and $_{276}$GILGYTEDDVVSTDFVGDNR, were ethylene-suppressed significantly to −2.12- and −1.95-fold, respectively (Table S6b), suggesting that ethylene regulates both the protein level and conformation of GAPC1. The third example is that the cross-linked peptide $_{384}$LKNVPIGVTA−$_{361}$TQVAYGSKNEIIR derived from sedoheptulose-bisphosphatase (SBPase, AT3G55800) had a 4.89-fold increase, whereas the linear peptide $_{291}$YTGGMVPDVNQIIVKEK from the same protein was insignificantly altered upon ethylene hormone treatment (Table S6b). Given that SBPase is an enzyme involved in the Calvin cycle and photosynthetic carbon fixation,[108] the breaking and forming of the disulfide bond between the Cys165 and Cys170 of wheat SBPase resulted in its structural changes, leading to activation and deactivation of this enzyme.[109] These two Cys are conserved between wheat and *Arabidopsis* SBPases. Ethylene has a crosstalk with hydrogen peroxide (H_2O_2),[110,111] and H_2O_2 is involved in the homeostasis of protein thiol redox in *Arabidopsis*;[112] we hereby hypothesize that the ethylene-induced structural change in SBPase is caused by a redox alteration of disulfide bonds in this enzyme induced by ethylene and H_2O_2 crosstalk. Of course, the alternative possibility would be that ethylene regulates the post-translational modification on SBPase (e.g., acetylation on K368 of SBPase[77]), which consequently altered the structure of SBPase. Consistent with the previous findings that ethylene regulates photosynthesis,[113,114] our quantitative interactomics study has further confirmed that ethylene regulates the protein structures of the light-harvesting complex of photosystem II 5 (LHCB5, AT4G10340) and RuBisCO small subunit 1B/2B/3B (RBCS1B/2B/3B, AT5G38430/AT5G38420/AT5G38410) (Table S6b) in addition to the novel finding on SBPase. It is therefore likely that ethylene may alter the protein structure to either an active or inactive state of these photosynthesis-related enzymes via altering both thiol redox and post-translational modification.

In conclusion, to identify in vivo protein−protein interactions and protein structure alteration in *Arabidopsis*, we have developed an IPQCX−MS workflow. Preliminary quantitative analysis of cross-linked peptides provided a means to monitor a limited change of interactomes in responding to a signal at the organismal level. This MS-based quantitative interactomics may be applied to the study of protein−protein interactions and protein structures of various crop plants and that between host and pathogen interactions.

■ ASSOCIATED CONTENT

Supporting Information

The Supporting Information is available free of charge on the ACS Publications website at DOI: 10.1021/acs.jproteome.8b00320.

Figure S1. MS spectrum of cross-linker AMDPS. Figure S2. MS spectrum of disulfide-linked biotin and alkyne (DLBA). Figure S3. MS^2 spectra of intermediate products (1), (2), (3), and the final product of cross-linked synthetic peptides EAKELIEGLPR and KELDDLR shown in Figure 1C. Figure S4. Two Venn diagrams of identified PSMs from *pLink*, *Kojak*, and ECL2. Figure S5. Verification of *phb3* T-DNA insertion line (SALK_020707) and *phb6* T-DNA insertion line (CS858159) using PCR. Figure S6. Workflow of wet lab. Figure S7. Comparison of the results of Gene Ontology (GO) analysis between the cross-linked proteins and the leaf proteome of *Arabidopsis*. Figure S8. Ethylene production rate of 38 day old *Arabidopsis* and ethylene effects on the phenotypes of 38 day old wild-type *Arabidopsis* Col-0 and mutant ein3/eil1. Figure S9. Validation of anti-PHB6 and PHB3 antibodies on 21 day old Col-0, phb3, phb6, and ein3/eil1. Figure S10. Calibration of the volumes of preserum used as negative control for coimmunoprecipitation. Figure S11. Titration and mutant experiments using anti-PHB3 antibody. Figure S12. Titration and mutant experiments using anti-PHB6 antibody. Figure S13. Super-resolution imaging of PHB3 and PHB6. Figure S14. Super-resolution imaging of PHB3 and PIP2a. Figure S15. Super-resolution imaging of PHB6 and PIP2a. Figure S16. Comparison of rosette diameters between *Col-0* and *phb6* mutants. (PDF)

Table S1a. Published software used to identify the cross-linked peptides that were generated by MS-noncleavable cross-linkers. Table S1b. Published software used to identify cross-linked peptides that were generated by MS-cleavable cross-linkers. (XLSX)

Table S2a. All PSMs of AMDSP monolinked peptides with FDR ≤ 0.01. Table S2b. Table containing all unique AMDSP monolinked peptides from Table S2a. Table S2c. Cellular components analysis of AMDSP monolinked proteins. (XLSX)

Table S3a. All PSMs of cross-linked peptides with FDR ≤ 0.05. Table S3b. All unique cross-linked peptides from Table S3a. Table S3c. All PSMs of cross-linked peptides with FDR ≤ 0.01. (XLSX)

Table S4. Quantification results. (XLSX)

Table S5. Biological processes and cellular components enrichment analysis of cross-linked proteins using AMDSP, DSBSO, or PIR containing cross-linker-based cross-linking, respectively. (XLSX)

Table S6a. Non-cross-linked (linear) peptides whose proteins have been used to quantify the cross-linked peptides in Table S4. Table S6b. Comparison of ethylene-regulated fold change of non-cross-linked (linear) peptide and cross-linked peptide from the same protein. (XLSX)

Supplemental File. Parameter files, log files, and results from *pLink*, *Kojak*, and ECL2, respectively.(ZIP)

■ AUTHOR INFORMATION

Corresponding Authors

*N.L.: E-mail: boningli@ust.hk. Tel: +852-23587335.
*W.Y.: E-mail: eeyu@ust.hk.

ORCID

Shichang Liu: 0000-0002-0251-5898
Fengchao Yu: 0000-0002-7695-3698

DOI: 10.1021/acs.jproteome.8b00320
J. Proteome Res. 2018, 17, 3195−3213

Author Contributions

S.L. conducted plant growth measurements and hormone treatment, protein isolation, peptide preparation, proteomics-related experiments, and immunoblot analysis. F.Y. and T.W. performed preliminary MS data analysis. F.Y., W.Y., and N.L. performed extensive MS data analysis. Q.H. and S.L. contributed to chemical reaction of synthetic peptides. F.Y., W.Y., and N.L. contributed to the establishment of ECL2 software coupled to a quantification module. S.D. provided the home-built super-resolution microscope. S.L., L.Y., and S.D. participated in super-resolution microscopy study. L.Y. and S.D. performed the colocalization coefficiency analysis. N.L., S.L., and F.Y. wrote the manuscript. N.L. supervised the project planning, the experimental design, the project execution, the coordination with multiple authors, and the communication with collaborators and was responsible for distribution of materials integral to the findings.

Author Contributions

○S.L. and F.Y. contributed equally to this work.

Notes

The authors declare no competing financial interest.

The mass spectrometry data have been deposited to the ProteomeXchange[83] Consortium via the PRIDE[84] partner repository with a data set identifier PXD008161.

■ ACKNOWLEDGMENTS

This work is mainly supported by grants 31370315, 31570187 (National Science Foundation of China), GDST16SC02, 661613, 16101114, 16103615, 16103817, AoE/M-403/16 (RGC of Hong Kong), SRF11EG17PG-A, SRFI11EG17-A (the HKUST internal support from the Energy Institute of HKUST), SBI09/10.EG01-A (the Croucher Foundation CAS-HKUST Joint Laboratory matching fund), GMGS14SC01, FP704, IRS18SC17, UROP17SC04, NMESL11SC01, PD13SC01, and VPRGO17SC07PG. T.W. acknowledges the support from Dr. Shun Tak Wu's Medical Sciences Fund to this work. S.D. acknowledges the support from the Offices of the Provost, VPRG and Dean of Science, HKUST (VPRGO12SC02), and Hong Kong Research Grants Council (C6030-14E) to this work. L.Y. acknowledges the support from Shuhuai Yao at Department of Mechanical and Aerospace Engineering, HKUST to this work. We thank Dr. Haiteng Deng and Miss Zhongyuan Sun for the technical support during LC–MS analysis. We thank Miss Marie Beatrix Kruth and Mr. Hang Shing Cheng for validation of ethylene-induced phenotype changes of plants. The super-resolution imaging software was provided by NanoBioImaging, Ltd.

■ REFERENCES

(1) Drewes, G.; Bouwmeester, T. Global approaches to protein–protein interactions. *Curr. Opin. Cell Biol.* **2003**, *15*, 199–205.

(2) Kelly, W.; Stumpf, M. Protein–protein interactions: from global to local analyses. *Curr. Opin. Biotechnol.* **2008**, *19*, 396–403.

(3) Mosca, R.; Pons, T.; Céol, A.; Valencia, A.; Aloy, P. Towards a detailed atlas of protein–protein interactions. *Curr. Opin. Struct. Biol.* **2013**, *23*, 929–940.

(4) Braun, P.; Aubourg, S.; Van Leene, J.; De Jaeger, G.; Lurin, C. Plant protein interactomes. *Annu. Rev. Plant Biol.* **2013**, *64*, 161–187.

(5) Kim, D. I.; Roux, K. J. Filling the void: proximity-based labeling of proteins in living cells. *Trends Cell Biol.* **2016**, *26*, 804–817.

(6) Mehla, J.; Caufield, J. H.; Uetz, P. The yeast two-hybrid system: A tool for mapping protein–protein interactions. *Cold Spring Harbor Protocols* **2015**, *2015*, pdb.top083345.

(7) St-Denis, N.; Gupta, G. D.; Lin, Z. Y.; Gonzalez-Badillo, B.; Pelletier, L.; Gingras, A.-C. Myotubularin-related proteins 3 and 4 interact with polo-like kinase 1 and centrosomal protein of 55 kDa to ensure proper abscission. *Mol. Cell. Proteomics* **2015**, *14*, 946–960.

(8) Popescu, S. C.; Popescu, G. V.; Bachan, S.; Zhang, Z.; Gerstein, M.; Snyder, M.; Dinesh-Kumar, S. P. MAPK target networks in Arabidopsis thaliana revealed using functional protein microarrays. *Genes Dev.* **2009**, *23*, 80–92.

(9) Kerppola, T. K. Bimolecular fluorescence complementation (BiFC) analysis as a probe of protein interactions in living cells. *Annu. Rev. Biophys.* **2008**, *37*, 465–487.

(10) Fujikawa, Y.; Kato, N. Technical advance: Split luciferase complementation assay to study protein–protein interactions in Arabidopsis protoplasts. *Plant J.* **2007**, *52*, 185–195.

(11) Gadella, T. W.; van der Krogt, G. N.; Bisseling, T. GFP-based FRET microscopy in living plant cells. *Trends Plant Sci.* **1999**, *4*, 287–291.

(12) Xu, X.; Soutto, M.; Xie, Q.; Servick, S.; Subramanian, C.; von Arnim, A. G.; Johnson, C. H. Imaging protein interactions with bioluminescence resonance energy transfer (BRET) in plant and mammalian cells and tissues. *Proc. Natl. Acad. Sci. U. S. A.* **2007**, *104*, 10264–10269.

(13) Rhee, H.-W.; Zou, P.; Udeshi, N. D.; Martell, J. D.; Mootha, V. K.; Carr, S. A.; Ting, A. Y. Proteomic mapping of mitochondria in living cells via spatially restricted enzymatic tagging. *Science* **2013**, *339*, 1328–1331.

(14) Roux, K. J.; Kim, D. I.; Raida, M.; Burke, B. A promiscuous biotin ligase fusion protein identifies proximal and interacting proteins in mammalian cells. *J. Cell Biol.* **2012**, *196*, 801–810.

(15) Youn, J.-Y.; Dunham, W. H.; Hong, S. J.; Knight, J. D.; Bashkurov, M.; Chen, G. I.; Bagci, H.; Rathod, B.; MacLeod, G.; Eng, S. W.; et al. High-density proximity mapping reveals the subcellular organization of mRNA-associated granules and bodies. *Mol. Cell* **2018**, *69*, 517–532.e11 e11.

(16) Trnka, M. J.; Burlingame, A. Topographic studies of the groel-groes chaperonin complex by chemical cross-linking using diformyl ethynylbenzene the power of high resolution electron transfer dissociation for determination of both peptide sequences and their attachment sites. *Mol. Cell. Proteomics* **2010**, *9*, 2306–2317.

(17) Leitner, A.; Reischl, R.; Walzthoeni, T.; Herzog, F.; Bohn, S.; Förster, F.; Aebersold, R. Expanding the chemical cross-linking toolbox by the use of multiple proteases and enrichment by size exclusion chromatography. *Mol. Cell. Proteomics* **2012**, *11*, M111.014126.

(18) Liu, F.; Heck, A. J. Interrogating the architecture of protein assemblies and protein interaction networks by cross-linking mass spectrometry. *Curr. Opin. Struct. Biol.* **2015**, *35*, 100–108.

(19) Herzog, F.; Kahraman, A.; Boehringer, D.; Mak, R.; Bracher, A.; Walzthoeni, T.; Leitner, A.; Beck, M.; Hartl, F.-U.; Ban, N.; et al. Structural probing of a protein phosphatase 2A network by chemical cross-linking and mass spectrometry. *Science* **2012**, *337*, 1348–1352.

(20) Leitner, A.; Faini, M.; Stengel, F.; Aebersold, R. Crosslinking and mass spectrometry: an integrated technology to understand the structure and function of molecular machines. *Trends Biochem. Sci.* **2016**, *41*, 20–32.

(21) Narain, R. *Chemistry of Bioconjugates: Synthesis, Characterization, and Biomedical Applications*; John Wiley & Sons Press: New York, 2013; pp 3–12.

(22) Chavez, J. D.; Schweppe, D. K.; Eng, J. K.; Bruce, J. E. In vivo conformational dynamics of Hsp90 and its interactors. *Cell Chemical Biology* **2016**, *23*, 716–726.

(23) Robinson, P. J.; Trnka, M. J.; Bushnell, D. A.; Davis, R. E.; Mattei, P.-J.; Burlingame, A. L.; Kornberg, R. D. Structure of a complete mediator-RNA polymerase II pre-initiation complex. *Cell* **2016**, *166*, 1411–1422 e16.

(24) Tang, X.; Bruce, J. E. A new cross-linking strategy: protein interaction reporter (PIR) technology for protein–protein interaction studies. *Mol. BioSyst.* **2010**, *6*, 939–947.

(25) Zhang, H.; Tang, X.; Munske, G. R.; Tolic, N.; Anderson, G. A.; Bruce, J. E. Identification of protein-protein interactions and topologies

DOI: 10.1021/acs.jproteome.8b00320
J. Proteome Res. 2018, 17, 3195–3213

in living cells with chemical cross-linking and mass spectrometry. *Mol. Cell. Proteomics* **2009**, *8*, 409−420.
(26) Zheng, C.; Yang, L.; Hoopmann, M. R.; Eng, J. K.; Tang, X.; Weisbrod, C. R.; Bruce, J. E. Cross-linking measurements of in vivo protein complex topologies. *Mol. Cell. Proteomics* **2011**, *10*, M110.006841.
(27) Schweppe, D. K.; Harding, C.; Chavez, J. D.; Wu, X.; Ramage, E.; Singh, P. K.; Manoil, C.; Bruce, J. E. Host-microbe protein interactions during bacterial infection. *Chem. Biol.* **2015**, *22*, 1521−1530.
(28) Kaake, R. M.; Wang, X.; Burke, A.; Yu, C.; Kandur, W.; Yang, Y.; Novtisky, E. J.; Second, T.; Duan, J.; Kao, A.; et al. A new in vivo cross-linking mass spectrometry platform to define protein−protein interactions in living cells. *Mol. Cell. Proteomics* **2014**, *13*, 3533−3543.
(29) Sinz, A. Crosslinking Mass Spectrometry Goes In-Tissue. *Cell Systems* **2018**, *6*, 10−12.
(30) Chavez, J. D.; Lee, C. F.; Caudal, A.; Keller, A.; Tian, R.; Bruce, J. E. Chemical Crosslinking Mass Spectrometry Analysis of Protein Conformations and Supercomplexes in Heart Tissue. *Cell Systems* **2018**, *6*, 136−141.e5.
(31) Zhu, X.; Yu, F.; Yang, Z.; Liu, S.; Dai, C.; Lu, X.; Liu, C.; Yu, W.; Li, N. In planta chemical cross-linking and mass spectrometry analysis of protein structure and interaction in Arabidopsis. *Proteomics* **2016**, *16*, 1915−1927.
(32) Wink, M. Introduction: Biochemistry, Physiology and Ecological Functions of Secondary Metabolites. In *Biochemistry of Plant Secondary Metabolism*, 2nd ed; Annual Plant Reviews *40*; Blackwell Publishing Press: Oxford, U.K., 2010; pp 1−19.
(33) Greber, B. J.; Boehringer, D.; Leitner, A.; Bieri, P.; Voigts-Hoffmann, F.; Erzberger, J. P.; Leibundgut, M.; Aebersold, R.; Ban, N. Architecture of the large subunit of the mammalian mitochondrial ribosome. *Nature* **2014**, *505*, 515−519.
(34) Walzthoeni, T.; Leitner, A.; Stengel, F.; Aebersold, R. Mass spectrometry supported determination of protein complex structure. *Curr. Opin. Struct. Biol.* **2013**, *23*, 252−260.
(35) Nguyen, V. Q.; Ranjan, A.; Stengel, F.; Wei, D.; Aebersold, R.; Wu, C.; Leschziner, A. E. Molecular architecture of the ATP-dependent chromatin-remodeling complex SWR1. *Cell* **2013**, *154*, 1220−1231.
(36) Pfaff, J.; Hennig, J.; Herzog, F.; Aebersold, R.; Sattler, M.; Niessing, D.; Meister, G. Structural features of Argonaute−GW182 protein interactions. *Proc. Natl. Acad. Sci. U. S. A.* **2013**, *110*, E3770−E3779.
(37) Zybailov, B.; Gokulan, K.; Wiese, J.; Ramanagoudr-Bhojappa, R.; Byrd, A. K.; Glazko, G.; Jaiswal, M.; Mackintosh, S.; Varughese, K. I.; Raney, K. D. Analysis of Protein-protein Interaction Interface between Yeast Mitochondrial Proteins Rim1 and Pif1 Using Chemical Cross-linking Mass Spectrometry. *J. Proteomics Bioinf.* **2015**, *8*, 243−252.
(38) Makowski, M. M.; Willems, E.; Jansen, P. W.; Vermeulen, M. Cross-linking immunoprecipitation-MS (xIP-MS): topological analysis of chromatin-associated protein complexes using single affinity purification. *Mol. Cell. Proteomics* **2016**, *15*, 854−865.
(39) Chu, F.; Maynard, J. C.; Chiosis, G.; Nicchitta, C. V.; Burlingame, A. L. Identification of novel quaternary domain interactions in the Hsp90 chaperone, GRP94. *Protein Sci.* **2006**, *15*, 1260−1269.
(40) Rinner, O.; Seebacher, J.; Walzthoeni, T.; Mueller, L.; Beck, M.; Schmidt, A.; Mueller, M.; Aebersold, R. Identification of cross-linked peptides from large sequence databases. *Nat. Methods* **2008**, *5*, 315−318.
(41) Walzthoeni, T.; Claassen, M.; Leitner, A.; Herzog, F.; Bohn, S.; Förster, F.; Beck, M.; Aebersold, R. False discovery rate estimation for cross-linked peptides identified by mass spectrometry. *Nat. Methods* **2012**, *9*, 901−903.
(42) Yang, B.; Wu, Y.-J.; Zhu, M.; Fan, S.-B.; Lin, J.; Zhang, K.; Li, S.; Chi, H.; Li, Y.-X.; Chen, H.-F.; He, S.-M.; Dong, M.-Q.; et al. Identification of cross-linked peptides from complex samples. *Nat. Methods* **2012**, *9*, 904−906.
(43) Hoopmann, M. R.; Zelter, A.; Johnson, R. S.; Riffle, M.; MacCoss, M. J.; Davis, T. N.; Moritz, R. L. Kojak: efficient analysis of chemically cross-linked protein complexes. *J. Proteome Res.* **2015**, *14*, 2190−2198.
(44) Yu, F.; Li, N.; Yu, W. ECL: an exhaustive search tool for the identification of cross-linked peptides using whole database. *BMC Bioinf.* **2016**, *17*, 1−8.
(45) Yu, F.; Li, N.; Yu, W. Exhaustively Identifying Cross-Linked Peptides with a Linear Computational Complexity. *J. Proteome Res.* **2017**, *16*, 3942−3952.
(46) Kao, A.; Chiu, C.-l.; Vellucci, D.; Yang, Y.; Patel, V. R.; Guan, S.; Randall, A.; Baldi, P.; Rychnovsky, S. D.; Huang, L. Development of a novel cross-linking strategy for fast and accurate identification of cross-linked peptides of protein complexes. *Mol. Cell. Proteomics* **2011**, *10*, M110.002212.
(47) Kao, A.; Randall, A.; Yang, Y.; Patel, V. R.; Kandur, W.; Guan, S.; Rychnovsky, S. D.; Baldi, P.; Huang, L. Mapping the structural topology of the yeast 19S proteasomal regulatory particle using chemical cross-linking and probabilistic modeling. *Mol. Cell. Proteomics* **2012**, *11*, 1566−1577.
(48) Clifford-Nunn, B.; Showalter, H. H.; Andrews, P. C. Quaternary diamines as mass spectrometry cleavable crosslinkers for protein interactions. *J. Am. Soc. Mass Spectrom.* **2012**, *23*, 201−212.
(49) Liu, F.; Rijkers, D. T.; Post, H.; Heck, A. J. Proteome-wide profiling of protein assemblies by cross-linking mass spectrometry. *Nat. Methods* **2015**, *12*, 1179−1184.
(50) Götze, M.; Pettelkau, J.; Fritzsche, R.; Ihling, C. H.; Schäfer, M.; Sinz, A. Automated assignment of MS/MS cleavable cross-links in protein 3D-structure analysis. *J. Am. Soc. Mass Spectrom.* **2015**, *26*, 83−97.
(51) Schmidt, C.; Zhou, M.; Marriott, H.; Morgner, N.; Politis, A.; Robinson, C. V. Comparative cross-linking and mass spectrometry of an intact F-type ATPase suggest a role for phosphorylation. *Nat. Commun.* **2013**, *4*, 1985.
(52) Tomko, R. J.; Taylor, D. W.; Chen, Z. A.; Wang, H.-W.; Rappsilber, J.; Hochstrasser, M. A single α helix drives extensive remodeling of the proteasome lid and completion of regulatory particle assembly. *Cell* **2015**, *163*, 432−444.
(53) Walzthoeni, T.; Joachimiak, L. A.; Rosenberger, G.; Röst, H. L.; Malmström, L.; Leitner, A.; Frydman, J.; Aebersold, R. xTract: software for characterizing conformational changes of protein complexes by quantitative cross-linking mass spectrometry. *Nat. Methods* **2015**, *12*, 1185−1190.
(54) Chen, Z. A.; Pellarin, R.; Fischer, L.; Sali, A.; Nilges, M.; Barlow, P. N.; Rappsilber, J. Structure of complement C3 (H2O) revealed by quantitative cross-linking/mass spectrometry and modeling. *Mol. Cell. Proteomics* **2016**, *15*, 2730−2743.
(55) Chavez, J. D.; Liu, N. L.; Bruce, J. E. Quantification of Protein−Protein Interactions with Chemical Cross-Linking and Mass Spectrometry. *J. Proteome Res.* **2011**, *10*, 1528−1537.
(56) Chavez, J. D.; Schweppe, D. K.; Eng, J. K.; Zheng, C.; Taipale, A.; Zhang, Y.; Takara, K.; Bruce, J. E. Quantitative interactome analysis reveals a chemoresistant edgotype. *Nat. Commun.* **2015**, *6*, 7928.
(57) Hsu, J.-L.; Huang, S.-Y.; Chow, N.-H.; Chen, S.-H. Stable-isotope dimethyl labeling for quantitative proteomics. *Anal. Chem.* **2003**, *75*, 6843−6852.
(58) Boersema, P. J.; Raijmakers, R.; Lemeer, S.; Mohammed, S.; Heck, A. J. Multiplex peptide stable isotope dimethyl labeling for quantitative proteomics. *Nat. Protoc.* **2009**, *4*, 484−494.
(59) Zhou, Y.; Shan, Y.; Zhang, L.; Zhang, Y. Recent advances in stable isotope labeling based techniques for proteome relative quantification. *Journal of Chromatography A* **2014**, *1365*, 1−11.
(60) Lassowskat, I.; Hartl, M.; Hosp, F.; Boersema, P. J.; Mann, M.; Finkemeier, I. Dimethyl-labeling-based quantification of the lysine acetylome and proteome of plants. *Methods Mol. Biol.* **2017**, *1653*, 65−81.
(61) Gygi, S. P.; Rist, B.; Gerber, S. A.; Turecek, F.; Gelb, M. H.; Aebersold, R. Quantitative analysis of complex protein mixtures using isotope-coded affinity tags. *Nat. Biotechnol.* **1999**, *17*, 994−999.
(62) Ross, P. L.; Huang, Y. N.; Marchese, J. N.; Williamson, B.; Parker, K.; Hattan, S.; Khainovski, N.; Pillai, S.; Dey, S.; Daniels, S.; et al. Multiplexed protein quantitation in Saccharomyces cerevisiae using

DOI: 10.1021/acs.jproteome.8b00320
J. Proteome Res. 2018, 17, 3195−3213

amine-reactive isobaric tagging reagents. *Mol. Cell. Proteomics* **2004**, *3*, 1154−1169.
(63) Thompson, A.; Schäfer, J.; Kuhn, K.; Kienle, S.; Schwarz, J.; Schmidt, G.; Neumann, T.; Hamon, C. Tandem mass tags: a novel quantification strategy for comparative analysis of complex protein mixtures by MS/MS. *Anal. Chem.* **2003**, *75*, 1895−1904.
(64) Woo, J.; Han, D.; Wang, J. I.; Park, J.; Kim, H.; Kim, Y. Quantitative Proteomics Reveals Temporal Proteomic Changes in Signaling Pathways during BV2Mouse Microglial Cell Activation. *J. Proteome Res.* **2017**, *16*, 3419−3432.
(65) Fang, H.; Xiao, K.; Li, Y.; Yu, F.; Liu, Y.; Xue, B.; Tian, Z. Intact Protein Quantitation Using Pseudoisobaric Dimethyl Labeling. *Anal. Chem.* **2016**, *88*, 7198−7205.
(66) Kantawong, F.; Burgess, K. E.; Jayawardena, K.; Hart, A.; Burchmore, R. J.; Gadegaard, N.; Oreffo, R. O.; Dalby, M. J. Whole proteome analysis of osteoprogenitor differentiation induced by disordered nanotopography and mediated by ERK signalling. *Biomaterials* **2009**, *30*, 4723−4731.
(67) Ytterberg, A. J.; Peltier, J.-B.; Van Wijk, K. J. Protein profiling of plastoglobules in chloroplasts and chromoplasts. A surprising site for differential accumulation of metabolic enzymes. *Plant Physiol.* **2006**, *140*, 984−997.
(68) Huang, H.-J.; Tsai, M.-L.; Chen, Y.-W.; Chen, S.-H. Quantitative shot-gun proteomics and MS-based activity assay for revealing gender differences in enzyme contents for rat liver microsome. *J. Proteomics* **2011**, *74*, 2734−2744.
(69) Wang, F.; Chen, R.; Zhu, J.; Sun, D.; Song, C.; Wu, Y.; Ye, M.; Wang, L.; Zou, H. A fully automated system with online sample loading, isotope dimethyl labeling and multidimensional separation for high-throughput quantitative proteome analysis. *Anal. Chem.* **2010**, *82*, 3007−3015.
(70) Khidekel, N.; Ficarro, S. B.; Clark, P. M.; Bryan, M. C.; Swaney, D. L.; Rexach, J. E.; Sun, Y. E.; Coon, J. J.; Peters, E. C.; Hsieh-Wilson, L. C. Probing the dynamics of O-GlcNAc glycosylation in the brain using quantitative proteomics. *Nat. Chem. Biol.* **2007**, *3*, 339−348.
(71) Lemeer, S.; Jopling, C.; Gouw, J.; Mohammed, S.; Heck, A. J.; Slijper, M.; den Hertog, J. Comparative phosphoproteomics of zebrafish Fyn/Yes morpholino knockdown embryos. *Mol. Cell. Proteomics* **2008**, *7*, 2176−2187.
(72) Parker, B. L.; Palmisano, G.; Edwards, A. V.; White, M. Y.; Engholm-Keller, K.; Lee, A.; Scott, N. E.; Kolarich, D.; Hambly, B. D.; Packer, N. H.; et al. Quantitative N-linked glycoproteomics of myocardial ischemia and reperfusion injury reveals early remodeling in the extracellular environment. *Mol. Cell. Proteomics* **2011**, *10*, M110.006833.
(73) van Noort, V.; Seebacher, J.; Bader, S.; Mohammed, S.; Vonkova, I.; Betts, M. J.; Kühner, S.; Kumar, R.; Maier, T.; O'Flaherty, M.; et al. Cross-talk between phosphorylation and lysine acetylation in a genome-reduced bacterium. *Mol. Syst. Biol.* **2012**, *8*, 1−16.
(74) Cheng, P.-C.; Chang, H.-K.; Chen, S.-H. Quantitative nano-proteomics for protein complexes (QNanoPX) related to estrogen transcriptional action. *Mol. Cell. Proteomics* **2010**, *9*, 209−224.
(75) Lau, H.-T.; Suh, H. W.; Golkowski, M.; Ong, S.-E. Comparing SILAC-and stable isotope dimethyl-labeling approaches for quantitative proteomics. *J. Proteome Res.* **2014**, *13*, 4164−4174.
(76) Chowdhury, S. M.; Du, X.; Tolic, N.; Wu, S.; Moore, R. J.; Mayer, M. U.; Smith, R. D.; Adkins, J. N. Identification of cross-linked peptides after click-based enrichment using sequential collision-induced dissociation and electron transfer dissociation tandem mass spectrometry. *Anal. Chem.* **2009**, *81*, 5524−5532.
(77) Liu, S.; Yu, F.; Yang, Z.; Wang, T.; Xiong, H.; Chang, C.; Yu, W.; Li, N. Establishment of dimethyl labelling-based quantitative acetylproteomics in Arabidopsis. *Mol. Cell. Proteomics* **2018**, *17*, 1010−1027.
(78) Serino, G.; Su, H.; Peng, Z.; Tsuge, T.; Wei, N.; Gu, H.; Deng, X. W. Characterization of the last subunit of the Arabidopsis COP9 signalosome: implications for the overall structure and origin of the complex. *Plant Cell* **2003**, *15*, 719−731.
(79) Guo, G.; Li, N. Relative and accurate measurement of protein abundance using 15 N stable isotope labeling in Arabidopsis (SILIA). *Phytochemistry* **2011**, *72*, 1028−1039.
(80) Qing, D.; Yang, Z.; Li, M.; Wong, W. S.; Guo, G.; Liu, S.; Guo, H.; Li, N. Quantitative and functional phosphoproteomic analysis reveals that ethylene regulates water transport via the C-terminal phosphorylation of aquaporin PIP2; 1 in Arabidopsis. *Mol. Plant* **2016**, *9*, 158−174.
(81) Gilmore, J. M.; Kettenbach, A. N.; Gerber, S. A. Increasing phosphoproteomic coverage through sequential digestion by complementary proteases. *Anal. Bioanal. Chem.* **2012**, *402*, 711−720.
(82) Chambers, M. C.; Maclean, B.; Burke, R.; Amodei, D.; Ruderman, D. L.; Neumann, S.; Gatto, L.; Fischer, B.; Pratt, B.; Egertson, J.; et al. A cross-platform toolkit for mass spectrometry and proteomics. *Nat. Biotechnol.* **2012**, *30*, 918−920.
(83) Deutsch, E. W.; Csordas, A.; Sun, Z.; Jarnuczak, A.; Perez-Riverol, Y.; Ternent, T.; Campbell, D. S.; Bernal-Llinares, M.; Okuda, S.; Kawano, S.; et al. The ProteomeXchange consortium in 2017: supporting the cultural change in proteomics public data deposition. *Nucleic Acids Res.* **2017**, *45*, D1100−D1106.
(84) Vizcaíno, J. A.; Csordas, A.; Del-Toro, N.; Dianes, J. A.; Griss, J.; Lavidas, I.; Mayer, G.; Perez-Riverol, Y.; Reisinger, F.; Ternent, T.; et al. 2016 update of the PRIDE database and its related tools. *Nucleic Acids Res.* **2016**, *44*, D447−D456.
(85) Baerenfaller, K.; Hirsch-Hoffmann, M.; Svozil, J.; Hull, R.; Russenberger, D.; Bischof, S.; Lu, Q.; Gruissem, W.; Baginsky, S. pep2pro: a new tool for comprehensive proteome data analysis to reveal information about organ-specific proteomes in Arabidopsis thaliana. *Integrative Biology* **2011**, *3*, 225−237.
(86) Roy, A.; Kucukural, A.; Zhang, Y. I-TASSER: a unified platform for automated protein structure and function prediction. *Nat. Protoc.* **2010**, *5*, 725−738.
(87) Schneidman-Duhovny, D.; Inbar, Y.; Nussinov, R.; Wolfson, H. J. PatchDock and SymmDock: servers for rigid and symmetric docking. *Nucleic Acids Res.* **2005**, *33*, W363−W367.
(88) Serino, G.; Deng, X.-W. Protein coimmunoprecipitation in Arabidopsis. *Cold Spring Harbor Protocols* **2007**, *2007*, pdb.prot4683.
(89) Paciorek, T.; Sauer, M.; Balla, J.; Wiśniewska, J.; Friml, J. Immunocytochemical technique for protein localization in sections of plant tissues. *Nat. Protoc.* **2006**, *1*, 104−107.
(90) Zhao, T.; Wang, Y.; Zhai, Y.; Qu, X.; Cheng, A.; Du, S.; Loy, M. A user-friendly two-color super-resolution localization microscope. *Opt. Express* **2015**, *23*, 1879−1887.
(91) Manders, E.; Verbeek, F.; Aten, J. Measurement of co-localization of objects in dual-colour confocal images. *J. Microsc.* **1993**, *169*, 375−382.
(92) Johnson, W. E.; Li, C.; Rabinovic, A. Adjusting batch effects in microarray expression data using empirical Bayes methods. *Biostatistics* **2007**, *8*, 118−127.
(93) Rosner, B. *Fundamentals of Biostatistics*, 7th ed.; Cengage Learning Press: Boston, MA, 2010; pp 1−859.
(94) Benjamini, Y.; Hochberg, Y. Controlling the false discovery rate: a practical and powerful approach to multiple testing. *J. R. Stat. Soc., Ser. B* **1995**, *57*, 289−300.
(95) Chu, F.; Mahrus, S.; Craik, C. S.; Burlingame, A. L. Isotope-coded and affinity-tagged cross-linking (ICATXL): an efficient strategy to probe protein interaction surfaces. *J. Am. Chem. Soc.* **2006**, *128*, 10362−10363.
(96) Ulintz, P. J.; Yocum, A. K.; Bodenmiller, B.; Aebersold, R.; Andrews, P. C.; Nesvizhskii, A. I. Comparison of MS2-only, MSA, and MS2/MS3 methodologies for phosphopeptide identification. *J. Proteome Res.* **2009**, *8*, 887−899.
(97) Ting, L.; Rad, R.; Gygi, S. P.; Haas, W. MS3 eliminates ratio distortion in isobaric multiplexed quantitative proteomics. *Nat. Methods* **2011**, *8*, 937−940.
(98) Van Aken, O.; Pečenková, T.; Van De Cotte, B.; De Rycke, R.; Eeckhout, D.; Fromm, H.; De Jaeger, G.; Witters, E.; Beemster, G. T.; Inzé, D.; et al. Mitochondrial type-I prohibitins of Arabidopsis thaliana

DOI: 10.1021/acs.jproteome.8b00320
J. Proteome Res. 2018, 17, 3195−3213

are required for supporting proficient meristem development. *Plant J.* **2007**, *52*, 850−864.
(99) Piechota, J.; Bereza, M.; Sokołowska, A.; Suszyński, K.; Lech, K.; Jańska, H. Unraveling the functions of type II-prohibitins in Arabidopsis mitochondria. *Plant Mol. Biol.* **2015**, *88*, 249−267.
(100) Mishra, S.; Ande, S. R.; Nyomba, B. The role of prohibitin in cell signaling. *FEBS J.* **2010**, *277*, 3937−3946.
(101) Artal-Sanz, M.; Tavernarakis, N. Prohibitin and mitochondrial biology. *Trends Endocrinol. Metab.* **2009**, *20*, 394−401.
(102) Back, J. W.; Sanz, M. A.; de Jong, L.; de Koning, L. J.; Nijtmans, L. G.; de Koster, C. G.; Grivell, L. A.; van der Spek, H.; Muijsers, A. O. A structure for the yeast prohibitin complex: Structure prediction and evidence from chemical crosslinking and mass spectrometry. *Protein Sci.* **2002**, *11*, 2471−2478.
(103) Piechota, J.; Kolodziejczak, M.; Juszczak, I.; Sakamoto, W.; Janska, H. Identification and characterization of high molecular weight complexes formed by matrix AAA proteases and prohibitins in mitochondria of Arabidopsis thaliana. *J. Biol. Chem.* **2010**, *285*, 12512−12521.
(104) Bavelloni, A.; Piazzi, M.; Raffini, M.; Faenza, I.; Blalock, W. L. Prohibitin 2: At a communications crossroads. *IUBMB Life* **2015**, *67*, 239−254.
(105) Van Aken, O.; Whelan, J.; Van Breusegem, F. Prohibitins: mitochondrial partners in development and stress response. *Trends Plant Sci.* **2010**, *15*, 275−282.
(106) Christians, M. J.; Larsen, P. B. Mutational loss of the prohibitin AtPHB3 results in an extreme constitutive ethylene response phenotype coupled with partial loss of ethylene-inducible gene expression in Arabidopsis seedlings. *J. Exp. Bot.* **2007**, *58*, 2237−2248.
(107) Arabidopsis Interactome Mapping Consortium. Evidence for network evolution in an Arabidopsis interactome map. *Science* **2011**, *333*, 601−607.
(108) Liu, X.-L.; Yu, H.-D.; Guan, Y.; Li, J.-K.; Guo, F.-Q. Carbonylation and loss-of-function analyses of SBPase reveal its metabolic interface role in oxidative stress, carbon assimilation, and multiple aspects of growth and development in Arabidopsis. *Mol. Plant* **2012**, *5*, 1082−1099.
(109) Dunford, R. P.; Durrant, M. C.; Catley, M. A.; Dyer, T. A. Location of the redox-active cysteines in chloroplast sedoheptulose-1, 7-bisphosphatase indicates that its allosteric regulation is similar but not identical to that of fructose-1, 6-bisphosphatase. *Photosynth. Res.* **1998**, *58*, 221−230.
(110) Desikan, R.; Last, K.; Harrett-Williams, R.; Tagliavia, C.; Harter, K.; Hooley, R.; Hancock, J. T.; Neill, S. J. Ethylene-induced stomatal closure in Arabidopsis occurs via AtrbohF-mediated hydrogen peroxide synthesis. *Plant J.* **2006**, *47*, 907−916.
(111) Desikan, R.; Hancock, J. T.; Bright, J.; Harrison, J.; Weir, I.; Hooley, R.; Neill, S. J. A role for ETR1 in hydrogen peroxide signaling in stomatal guard cells. *Plant Physiol.* **2005**, *137*, 831−834.
(112) Hu, Q.; Guo, G.; Yang, Z.; Li, Y.; Xia, Y.; Li, N. Stable isotope metabolic labeling-based quantitative thiol redox proteomic analysis of hydrogen peroxide-treated Arabidopsis plant. *J. Proteomics Bioinf.* **2014**, *5*, 121−133.
(113) Kays, S.; Pallas, J., Jr Inhibition of photosynthesis by ethylene. *Nature* **1980**, *285*, 51−52.
(114) Tholen, D.; Pons, T. L.; Voesenek, L. A.; Poorter, H. Ethylene insensitivity results in down-regulation of Rubisco expression and photosynthetic capacity in tobacco. *Plant Physiol.* **2007**, *144*, 1305−1315.

DOI: 10.1021/acs.jproteome.8b00320
J. Proteome Res. 2018, 17, 3195−3213